eman ta zabal zazu

Universidad del País Vasco

Euskal Herriko Unibertsitatea

University Master's Degree in Mathematical, Statistical, and Computational Modeling and Research 2025/2026

Master's Thesis

Spectral Analysis of Second-Order Delay Differential Equations via the Cayley Transform: An Application to Machining Chatter

---

Andoni Uyarra Irigoyen

Supervisor:
Felipe Eduardo Ponce Vanegas (BCAM)

Place and date of scheduled presentation:
Leioa, Zientzia eta Teknologia Fakultatea, EHU
09/2026

Resumen

Las ecuaciones diferenciales con retardo (EDR) son omnipresentes en ingeniería y ciencia, pero su análisis de estabilidad es más complejo que el de las ecuaciones ordinarias, pues su generador infinitesimal es un operador no acotado con infinitas raíces características. Este trabajo desarrolla un método numérico para el análisis espectral directo de EDR lineales de segundo orden, extendiendo el marco de la transformada de Cayley de Irastorza-Zabalegi y Ponce-Vanegas —concebido originalmente para sistemas de primer orden— directamente al operador de segundo orden, sin necesidad de reformular el problema como un sistema aumentado de primer orden y dimensión $2n$. Se construyen el semigrupo C_0 y el generador del operador, se le adapta la transformada de Cayley, obteniendo una discretización de Galerkin con splines lineales. El algoritmo se implementa en Python y se valida numéricamente. El código está disponible en `https://gitlab.bcamath.org/auyarra/ddemultiple`, donde el README recoge más información. Contrariamente a la hipótesis inicial, el método directo no mejora la precisión del método de primer orden existente; sin embargo, es asintóticamente ocho veces más eficiente y, a diferencia de la formulación aumentada, reduce sustancialmente la generación de autovalores espurios. Finalmente, se aplica al problema del *chatter* regenerativo en mecanizado, reproduciendo con éxito los lóbulos de estabilidad clásicos de la literatura. Estos resultados consolidan el tratamiento directo de segundo orden como una alternativa computacionalmente superior para el análisis de EDR.

Abstract

Delay differential equations (DDEs) are omnipresent in engineering and science, yet their stability analysis is considerably more complicated than for ordinary differential equations, since the associated infinitesimal generator is unbounded and its spectrum consists of infinitely many characteristic roots. This thesis develops a numerical method for the direct spectral analysis of linear second-order DDEs, extending the first-order Cayley-transform framework of Irastorza-Zabalegi and Ponce-Vanegas to the non-augmented second-order space, instead of reformulating the problem as an equivalent $2n$-dimensional first-order system. We construct the C_0-semigroup and infinitesimal generator associated with the second-order operator, adapt the Cayley transform to it, and derive a Galerkin discretization based on linear splines. The resulting algorithm is implemented in Python and validated numerically. The code is available at `https://gitlab.bcamath.org/auyarra/ddemultiple`, where the README provides further information. Contrary to our initial hypothesis, the direct method does not improve on the accuracy of the existing first-order approach; however, it is eight times more computationally efficient and, unlike the augmented formulation, substantially reduces spurious eigenvalues. Finally, the algorithm is applied to the regenerative *chatter* problem in machining, successfully reproducing the classical stability lobes reported in the literature. These results establish the direct second-order treatment as a computationally superior alternative for the spectral analysis of second-order delay differential equations.

Contents

List of Figures

Chapter 1

Introduction

1.1 Motivation and Context

Delay differential equations (DDEs) describe dynamical systems whose evolution at a given time depends not only on the present state of the system, but also on its state at one or more instants in the past. This "memory" effect is the natural way of modelling processes in which information, energy or material takes a finite time to propagate: population dynamics with maturation periods, control systems with communication or actuation lags, laser dynamics, and, as discussed at the end of this thesis, the regenerative vibrations that arise in machining. Even when the underlying physical law is itself a second-order differential equation, as is the case throughout this work, the presence of a discrete delay $\tau > 0$ makes the associated initial-value problem infinite-dimensional: the natural state of the system at time t is not a vector in $\mathbb{C}^n$, but the pair formed by the recent history of the solution on $[t-\tau, t]$ together with its instantaneous value. Consequently, stability questions that are elementary for ordinary differential equations—reduced there to the sign of the real part of finitely many eigenvalues of a matrix—become more delicate for DDEs, since the associated infinitesimal generator is an unbounded operator whose spectrum consists of infinitely many roots of a characteristic equation.

The specific problem addressed in this thesis is posed directly at the second-order level. Given a linear second-order delay differential equation

$$u''(t) = A\,u'(t) + B\,u(t) + C\,u'(t-\tau) + D\,u(t-\tau),$$

where $A, B, C, D \in \mathbb{C}^{n\times n}$, $\tau > 0$ is the delay, and $u : [0, \infty) \to \mathbb{C}^n$. The standard approach in the literature is to rewrite it as an equivalent $2n$-dimensional first-order system, for which the semigroup and spectral theory of first-order DDEs is already well established, and to build a numerical method on top of that first-order formulation. Instead of following this route, the present work keeps the non-augmented second-order space and develops the semigroup, generator and Cayley-transform machinery directly for the second-order operator. This decision adds a layer of complexity to the theoretical effort required, since none of the first-order results can simply be inherited, but it avoids duplicating the dimension of the space—an advantage that is expected to translate into a computational gain, and whose verification is one of the goals of this thesis.

This work has been developed within the Master's Degree in Mathematical Modelling and Research in Mathematics, Statistics and Computation (*Máster Universitario en Modelización e Investigación Matemática, Estadística y Computación*) of the University of the Basque Country (EHU), and it draws directly on competences acquired in several of its courses. The qualitative theory of differential equations covered in *Ecuaciones en Derivadas Parciales* (Partial Differential Equations)—existence, uniqueness, well-posedness and long-time behaviour of solutions—underlies the semigroup-theoretic treatment of Chapter 2, even though the operator studied there acts on an ordinary, rather than a partial differential equation. The design and complexity comparison of competing numerical implementations, practised in *Computación Científica y Álgebra Computacional* (Scientific Computing and Computational Algebra), underlies the efficiency analysis of Sections 3.6 and 3.7, where the computational cost of the direct and augmented formulations is compared explicitly in terms of loop structure, matrix size and asymptotic scaling. The discretization, convergence and error-estimation techniques studied in *Métodos Numéricos en Física e Ingeniería* (Numerical Methods in Physics and Engineering) are applied throughout Chapter 3. Finally, the object-oriented Python programming skills developed in *Bases de Datos y Programación Orientada a Objetos* (Databases and Object-Oriented Programming) made possible the numerical implementation of the algorithm.

From an applied perspective, part of the motivation for this work stems from an internship carried out in collaboration with the Aeronautics Advanced Manufacturing Center (*Centro de Fabricación Avanzada Aeronáutica*, CFAA), during which the numerical method developed here was applied to a industrial stability problem: the prediction of chatter in machining processes, discussed in Section 3.9.

1.2 Background and State of the Art

The operator-theoretic treatment of the delay equation followed in this thesis rests on the theory of strongly continuous (C_0-)semigroups, as exposed for example in [8], building on the general functional-analytic foundations covered, for instance, in Kreyszig [5]. Within this framework, the spectral theory specific to delay equations—the identification of the spectrum of the infinitesimal generator with the roots of a characteristic equation, together with the associated results on the distribution of these roots and on exponential stability—follows the classical exposition of Lunel [7].

On the numerical side, a standard family of methods for approximating the spectrum of a DDE is semi-discretization, thoroughly developed by Insperger and Stépán [3] and based, in essence, on discretizing the exponential solution operator; because the complex exponential map is periodic, it is not injective, which can compromise a faithful recovery of the spectrum. More recently, Irastorza-Zabalegi and Ponce-Vanegas [4] proposed an alternative for first-order delay systems based on the Cayley transform—known in numerical-analysis contexts as the Tustin method or bilinear transform—which maps the unbounded infinitesimal generator into a bounded operator through a one-to-one mapping, and combined it with a Galerkin discretization to obtain a numerically tractable generalized eigenvalue problem. This first-order Cayley-transform method is the direct starting point and the main point of comparison of the present thesis, which extends the same underlying idea to the second-order operator, avoiding the need to augment the space.

On the applied side, delay differential equations have long been used to model the regenerative effect responsible for machine-tool chatter, whose origin and historical development are reviewed in Section 3.9.1. To validate the proposed method against a well-documented engineering problem, Section 3.9 adopts the one-degree-of-freedom turning model and stability-lobe construction described by Insperger and Stépán [2].

1.3 Objectives

The main objective of this thesis is to develop and implement a numerical method for the direct spectral analysis of linear second-order delay differential equations that is computationally more efficient than the existing approach, which consists of reformulating the problem as an augmented first-order system and applying the Cayley-transform method of Irastorza-Zabalegi and Ponce-Vanegas [4]. This is complemented by an applied objective, motivated by an internship carried out in collaboration with the Aeronautics Advanced Manufacturing Center (CFAA): to demonstrate the practical relevance of the resulting algorithm on a real engineering problem, the prediction of regenerative chatter in machining.

These two objectives are pursued through the following specific goals:

1. Construct, directly from the second-order delay differential equation, the associated C_0-semigroup and its infinitesimal generator A_2, and establish the relationship between the spectrum of A_2 and the roots of the corresponding characteristic equation (Chapter 2).

2. Adapt the Cayley transform to this second-order operator and derive a Galerkin discretization, based on linear splines, of the resulting bounded operator (Chapter 2).

3. Implement the algorithm in Python and assess, empirically, its computational cost against the augmented first-order approach (Chapter 3).

4. Apply the resulting algorithm to the regenerative chatter problem in a turning process, validating it against the classical stability lobes reported in the machining literature (Chapter 3).

1.4 Methodology

The work was supervised through weekly meetings with the thesis advisor, in which progress was reviewed, intermediate results were validated, and the following steps were planned. Around these regular meetings, the work itself was organized into four stages. First, a literature review was carried out on the functional-analytic background of semigroup theory [8, 5], on the spectral theory of delay equations [7], on semi-discretization methods [3], and, in particular, on the first-order Cayley-transform method of [4] that this thesis extends. Second, building on this theoretical basis, the operator-theoretic framework of Chapter 2 was derived and implemented as a Python algorithm, using Git for version control. Third, the implementation was checked for coherence, by verifying that the computed spectra reproduced the qualitative behaviour predicted by the theory—for instance, the mapping of the stability boundary onto the unit circle and the accumulation of the highly damped part of the spectrum at -1 under the Cayley transform. Finally, once the implementation was deemed reliable, numerical tests were carried out—convergence studies, comparison against the augmented first-order approach, and the machining-chatter application—from which the conclusions of Chapter 4 were drawn.

1.5 Structure of the Thesis

The remainder of this thesis is organized as follows. Chapter 2 develops the theoretical framework of the method. Section 2.3 formulate the second-order delay differential equation, construct the associated C_0-semigroup $\{T_2(s)\}_{s\geq 0}$ and its infinitesimal generator A_2, and establish the equivalence between the exponential stability of the system and the location of the roots of its characteristic equation. Sections 2.4 and 2.5 introduce the Cayley transform of A_2 and its Galerkin discretization by linear splines, exploiting a subspace decomposition that keeps the resulting matrices sparse. Section 2.6 discusses the normalization of the delay to $\tau = 1$. Chapter 3 presents the numerical case studies. The method is first validated against the known spectral properties of the Cayley transform (Sections 3.1 and 3.2), and its convergence is analyzed as a function of the mesh size and of the dimension of the system (Sections 3.3 and 3.4). Sections 3.5–3.8 compare the proposed direct second-order method with the augmented first-order approach of [4], in terms of accuracy, computational cost and spectral purity, showing the eightfold reduction in computational cost achieved by avoiding the duplicated space. Finally, Section 3.9 applies the method to the regenerative chatter problem in turning processes, reproducing the classical stability lobes of [2]. Chapter 4 gathers the conclusions of the thesis, discussing the strengths and limitations of the proposed approach and possible directions for future work.

Chapter 2

Problem statement and formulation

2.1 The semigroup point of view

We consider the following second-order delay differential equation:

$$u''(t) = Au'(t) + Bu(t) + Cu'(t - \tau) + Du(t - \tau), \tag{2.1}$$

where $A, B, C, D \in \mathbb{C}^{n\times n}$, $\tau > 0$ is the delay, and $u : [0, \infty) \to \mathbb{C}^n$. To make sense of this equation when $t \in [0, \tau)$ we have to extend u to $[-\tau, 0)$ using some initial data ϕ defined in $[-\tau, 0]$.

Having formulated the delay differential equation (2.1) together with its initial data, we now recast the problem within an operator-theoretic framework. We begin by introducing a suitable Banach space on which the equation can be reformulated as an abstract evolution problem, together with a family of operators that advances a given pair of initial data forward in time along the corresponding solution. We then verify that this family satisfies the defining properties of a C_0-semigroup, and finally compute its infinitesimal generator explicitly; this generator will be the central object through which the stability of (2.1) is analysed in the remainder of this chapter.

The natural space on which to reformulate (2.1) is the Banach space

$$X = C^0([-\tau, 0], \mathbb{C}^n) \times \mathbb{C}^n, \tag{2.2}$$

which we equip with the norm

$$\|(\psi, v)\|_X := \|\psi\|_{C^0} + |v|, \qquad \|\psi\|_{C^0} := \sup_{\theta\in[-\tau,0]} |\psi(\theta)|, \tag{2.3}$$

where $|\cdot|$ denotes the Euclidean norm on $\mathbb{C}^n$: the first component of a pair $(\psi, v) \in X$ is measured in the supremum norm on $C^0([-\tau, 0], \mathbb{C}^n)$, while the second component is measured directly in the Euclidean norm on $\mathbb{C}^n$. Equipped with $\|\cdot\|_X$, the space X is indeed a Banach space, being the product of two Banach spaces.

An initial condition is specified by a pair $(\psi, v) \in X$, where $\psi \in C^0([-\tau,0],\, \mathbb{C}^n)$ and $v \in \mathbb{C}^n$. The corresponding initial function $\phi : [-\tau, 0] \to \mathbb{C}^n$ is defined by

$$\phi(t) = v + \int_{-\tau}^{t} \psi(\theta)\, d\theta, \qquad t \in [-\tau, 0], \tag{2.4}$$

so that $\phi'(t) = \psi(t)$ for all $t \in [-\tau, 0]$, and $\phi(-\tau) = v$.

With the space X and its norm fixed, we introduce the family of operators that describes the evolution of the system.

Definition 2.1.1. *For $s \geq 0$, the operator $T_2(s) : X \to X$ is defined as follows. Given $(\psi, v) \in X$, let u be the solution of* (2.1) *with initial condition given by* (2.4)*. Then*

$$T_2(s)(\psi,\, v) \;=\; (\psi_s,\, v_s), \tag{2.5}$$

where $\psi_s \in C^0([-\tau,0],\, \mathbb{C}^n)$ is defined by

$$\psi_s(t) = u'(s+t), \qquad t \in [-\tau, 0], \tag{2.6}$$

and $v_s = u(s-\tau) \in \mathbb{C}^n$.

We now check that the family $\{T_2(s)\}_{s\geq 0}$ just defined is indeed a semigroup in the precise sense required by the theory, namely a C_0-semigroup. We begin by recalling the definition.

Definition 2.1.2 ([8], Definition 2.1)**.** *Let X be a Banach space. A family $\{T(t)\}_{t\geq 0} \subset \mathcal{L}(X)$ of bounded linear operators on X is called a* strongly continuous semigroup *(or C_0-semigroup) if:*

(i) $T(0) = I$,

(ii) $T(t+s) = T(t)\,T(s)$ *for all* $t, s \geq 0$,

(iii) $\lim_{t\to 0^+} \|T(t)x - x\|_X = 0$ *for every* $x \in X$.

Proposition 2.1.1. *The family $\{T_2(s)\}_{s\geq 0}$ defined in Definition 2.1.1 is a C_0-semigroup on X.*

Proof. We verify the three properties of Definition 2.1.2.

Property (i): $T_2(0) = I$. By Definition 2.1.1,

$$T_2(0)(\psi, v) = (\psi_0,\, v_0), \tag{2.7}$$

where $\psi_0(t) = u'(0+t) = u'(t)$ for $t \in [-\tau, 0]$, and $v_0 = u(0-\tau) = u(-\tau)$. By the initial condition (2.4), $u'(t) = \phi'(t) = \psi(t)$ and $u(-\tau) = \phi(-\tau) = v$. Therefore $T_2(0)(\psi, v) = (\psi, v)$.

Property (ii): $T_2(t+s) = T_2(t)\,T_2(s)$. Let $(\psi, v) \in X$ be fixed, and let u be the corresponding solution of (2.1). We compute

$$T_2(s)(\psi, v) = (\psi_s,\, v_s), \qquad \psi_s(t) = u'(s+t),\; t \in [-\tau, 0], \qquad v_s = u(s-\tau). \tag{2.8}$$

We now apply $T_2(t)$ to (ψ_s, v_s). The solution $\widetilde{u}$ of (2.1) associated with initial condition (ψ_s, v_s) satisfies

$$\widetilde{\phi}(-\tau) = v_s = u(s-\tau), \qquad \widetilde{\phi}'(\theta) = \psi_s(\theta) = u'(s+\theta), \quad \theta \in [-\tau, 0]. \tag{2.9}$$

This is precisely the solution u shifted by s, namely $\widetilde{u}(\xi) = u(s+\xi)$. Applying Definition 2.1.1,

$$T_2(t)(\psi_s,\, v_s) = (\chi,\, w), \tag{2.10}$$

where $\chi(\theta) = \widetilde{u}'(t+\theta) = u'(s+t+\theta)$ for $\theta \in [-\tau, 0]$, and $w = \widetilde{u}(t-\tau) = u(s+t-\tau)$. This is exactly $T_2(s+t)(\psi, v)$, so $T_2(t)\, T_2(s) = T_2(t+s)$.

Property (iii): $\lim_{s\to 0^+} \|T_2(s)(\psi, v) - (\psi, v)\|_X = 0$ for every $(\psi, v) \in X$. Let $(\psi, v) \in X$ be fixed. By (2.5), $T_2(s)(\psi, v) = (\psi_s, v_s)$ with $\psi_s(t) = u'(s+t)$ and $v_s = u(s-\tau)$. By the norm defined in (2.3),

$$\|T_2(s)(\psi, v) - (\psi, v)\|_X = \|\psi_s - \psi\|_{C^0} + |v_s - v|, \tag{2.11}$$

so it suffices to show that each term on the right-hand side tends to 0 as $s \to 0^+$.

Second component. Since u is C^1, it is in particular continuous. As $s-\tau \to -\tau$ when $s \to 0^+$, continuity of u gives

$$\lim_{s\to 0^+} |u(s-\tau) - u(-\tau)| = 0, \qquad \text{i.e.} \qquad \lim_{s\to 0^+} u(s-\tau) = v. \tag{2.12}$$

First component. This term is of a different nature: it is a statement about convergence in the C^0-norm, so we must show that $u'(s+t)$ converges to $u'(t)$ *uniformly* on $[-\tau, 0]$, and not merely at each point of $[-\tau, 0]$ individually. As in the argument above, u' is continuous on the compact interval $[-\tau, \delta_0]$ for some $\delta_0 > 0$. By the Heine–Cantor theorem, a function that is continuous on a compact set is in fact *uniformly* continuous there; hence u' is uniformly continuous on $[-\tau, \delta_0]$. Explicitly, for every $\delta' > 0$ there exists $\varepsilon \in (0, \delta_0)$ such that

$$a, b \in [-\tau, \delta_0],\; |a-b| < \varepsilon \quad \Longrightarrow \quad |u'(a) - u'(b)| < \delta'. \tag{2.13}$$

Fix $\delta' > 0$ and let ε be as in (2.13). For $0 < s < \varepsilon$ and *any* $t \in [-\tau, 0]$, both t and $s+t$ lie in $[-\tau, \delta_0]$, and $|(s+t) - t| = s < \varepsilon$; therefore $|u'(s+t) - u'(t)| < \delta'$. The same ε works simultaneously for every $t \in [-\tau, 0]$, so

$$\|\psi_s - \psi\|_{C^0} = \sup_{t\in[-\tau,0]} |u'(s+t) - u'(t)| \le \delta' \qquad \text{whenever } 0 < s < \varepsilon. \tag{2.14}$$

Since $\delta' > 0$ was arbitrary, $\|\psi_s - \psi\|_{C^0} \to 0$ as $s \to 0^+$.

Combining both components in (2.11),

$$\lim_{s\to 0^+} \|T_2(s)(\psi, v) - (\psi, v)\|_X = 0 \qquad \text{for every } (\psi, v) \in X. \tag{2.15}$$

□

Having established that $\{T_2(s)\}_{s\geq 0}$ is a C_0-semigroup, we now turn to computing its infinitesimal generator, which will be the operator through which we relate the semigroup to the original delay equation and, ultimately, to its stability. We recall the definition of the infinitesimal generator of a C_0-semigroup.

Definition 2.1.3 ([8], Chapter 1.1)**.** *Let $\{T(t)\}_{t\geq 0}$ be a C_0-semigroup on a Banach space X. The* infinitesimal generator *of T is the operator $A : D(A) \subset X \to X$ defined by*

$$Ax = \lim_{h\to 0^+} \frac{T(h)x - x}{h}, \tag{2.16}$$

with domain $D(A)$ consisting of all $x \in X$ for which this limit exists in X.

2.1.1 The infinitesimal generator of T_2 and its domain

We denote by A_2 the infinitesimal generator of $\{T_2(s)\}_{s\geq 0}$ and proceed to prove the following important theorem.

Theorem 2.1.1. *The infinitesimal generator A_2 of the C_0-semigroup $\{T_2(s)\}_{s\geq 0}$ acts as*

$$A_2(\psi, v) = \big(\psi',\ \psi(-\tau)\big), \tag{2.17}$$

with domain

$$D(A_2) = \Big\{(\psi, v) \in C^1([-\tau, 0], \mathbb{C}^n) \times \mathbb{C}^n \ :\ \psi'(0) = \\ A\psi(0) + B\phi(0) + C\psi(-\tau) + Dv\Big\}, \tag{2.18}$$

where $\phi(t) = v + \int_{-\tau}^{t} \psi(\theta)\, d\theta$.

Proof. Let $(\psi, v) \in X$. By Definitions 2.1.1 and 2.1.3, we form the difference quotient

$$\frac{T_2(h)(\psi, v) - (\psi, v)}{h} = \left(\frac{\psi_h - \psi}{h},\ \frac{v_h - v}{h}\right), \tag{2.19}$$

where the first component is the function whose value at $t \in [-\tau, 0]$ is $\frac{u'(h+t)-\psi(t)}{h}$, and the second component is $\frac{u(h-\tau)-v}{h}$. Now, we will analyse each component separately, starting with the easiest part.

Second component of A_2: For $h < \tau$ we have $h - \tau \in (-\tau, 0)$, so $u(h - \tau) = \phi(h - \tau)$. Using the definition of ϕ in (2.4):

$$\phi(h - \tau) = v + \int_{-\tau}^{h-\tau} \psi(\theta)\, d\theta. \tag{2.20}$$

Subtracting v and dividing by h:

$$\frac{u(h - \tau) - v}{h} = \frac{1}{h}\int_{-\tau}^{-\tau+h} \psi(\theta)\, d\theta. \tag{2.21}$$

Define $F : [-\tau, 0] \to \mathbb{C}^n$ by

$$F(\xi) = \int_{-\tau}^{\xi} \psi(\theta)\, d\theta. \tag{2.22}$$

Since $\psi \in C^0([-\tau, 0], \mathbb{C}^n)$, the Fundamental Theorem of Calculus guarantees that F is differentiable and $F'(\xi) = \psi(\xi)$ for all $\xi \in [-\tau, 0]$. Noting that $F(-\tau) = 0$, the quotient becomes

$$\frac{1}{h}\int_{-\tau}^{-\tau+h} \psi(\theta)\, d\theta = \frac{F(-\tau + h) - F(-\tau)}{h} \xrightarrow{h\to 0^+} F'(-\tau) = \psi(-\tau). \tag{2.23}$$

The limit of the second component is therefore $\psi(-\tau)$.

First component of A_2: We now examine the limit $\frac{1}{h}(u'(h+t) - \psi(t))$. To begin with, let us assume that this limit exists in $C^0([-\tau, 0], \mathbb{C}^n)$; in particular, the limit exists pointwise. Let us fix $t \in [-\tau, 0)$ and assume that $h < |t|$, so we have $h + t \in (-\tau, 0)$ and $u'(h + t) = \phi'(h + t) = \psi(h + t)$. The difference quotient becomes

$$\frac{u'(h + t) - \psi(t)}{h} = \frac{\psi(h + t) - \psi(t)}{h} \xrightarrow{h\to 0^+} \psi'(t). \tag{2.24}$$

This requires ψ to be differentiable at these points.

When $t = 0$ we have $h + t = h > 0$, so $u'(h)$ must be determined by (2.1). The limit of the quotient is

$$\lim_{h\to 0^+} \frac{u'(h) - \psi(0)}{h} = u''(0^+). \tag{2.25}$$

Evaluating (2.1) at $t = 0^+$ and using $u'(0) = \phi'(0) = \psi(0)$, $u(0) = \phi(0)$, $u'(-\tau) = \phi'(-\tau) = \psi(-\tau)$, and $u(-\tau) = \phi(-\tau) = v$, we obtain

$$u''(0^+) = A\psi(0) + B\phi(0) + C\psi(-\tau) + Dv. \tag{2.26}$$

Recall that we are assuming that the limit $\frac{1}{h}(u'(h + t) - \psi(t))$ of the first component in (2.19) exists in $C^0([-\tau, 0], \mathbb{C}^n)$, so the limit function must be continuous at $t = 0$. Since the limit equals $\psi'(t)$ in $[-\tau, 0)$, then the value from the left $\psi'(0)$ must agree with the value at $t = 0$ computed above, giving the condition:

$$\psi'(0) = A\psi(0) + B\phi(0) + C\psi(-\tau) + Dv. \tag{2.27}$$

Again, since convergence is uniform, we also have that $\psi \in C^1([-\tau, 0], \mathbb{C}^n)$, which shows that the functions in $\mathcal{D}(A_2)$ belong to the set at the right of (2.18).

Conversely, assume that ψ belongs to the set at the right of (2.18), so we have to show that the limit $\frac{1}{h}(u'(h+t)-\psi(t))$ exists and is uniform in $t \in [-\tau, 0]$. By the arguments just given, we can see that the boundary condition (2.27) implies that u' is differentiable at $t = 0$. This, together with the conditions $\psi \in C^1([-\tau, 0], \mathbb{C}^n)$, implies that u'' is continuous in an interval $[-\tau, \delta]$ for some $\delta > 0$.

By the mean value theorem, $\frac{1}{h}(u'(h+t)-\psi(t)) = u''(\theta_t)$ for some $\theta_t \in (t, t+h)$. Then, for $h_1 < h_2 < \delta$ we have

$$\frac{1}{h_1}(u'(h_1+t)-\psi(t)) - \frac{1}{h_2}(u'(h_2+t)-\psi(t)) = u''(\theta_{1,t}) - u''(\theta_{2,t}). \tag{2.28}$$

Since u'' is continuous and $|\theta_{1,t}-\theta_{2,t}| < h_2$ for all $t \in [-\tau, 0]$, by uniform continuity we conclude that the limit exists and is uniform in t.

□

2.2 Connection with first-order DDEs

By defining the augmented state vector $y(t) = (u(t), u'(t))^T$, our second-order equation can be formally rewritten as a $2n$-dimensional first-order system:

$$\dot{y}(t) = B_0 y(t) + B_1 y(t-\tau), \tag{2.29}$$

where the block matrices are given by:

$$B_0 = \begin{pmatrix} 0 & I \\ B & A \end{pmatrix}, \qquad B_1 = \begin{pmatrix} 0 & 0 \\ D & C \end{pmatrix}. \tag{2.30}$$

Because this equivalence exists, all the theorems regarding the spectrum and asymptotic behavior of first-order DDEs apply to our system. However, in this work, we will not proceed with this dimensionally augmented system. We choose to work directly with the second-order operator A_2 and its natural space X. Preserving the original second-order structure prevents the duplication of the system's dimension, offering computational and numerical advantages later on.

To bridge the first-order theory with our second-order operator, we examine the characteristic matrix. Applying the standard definition for a first-order system [7], we obtain:

$$\Delta_{1\mathrm{st}}(z) = zI_{2n} - B_0 - B_1 e^{-z\tau}. \tag{2.31}$$

Substituting our specific block matrices yields:

$$\begin{aligned} \Delta_{1\mathrm{st}}(z) &= \begin{pmatrix} zI & 0 \\ 0 & zI \end{pmatrix} - \begin{pmatrix} 0 & I \\ B & A \end{pmatrix} - \begin{pmatrix} 0 & 0 \\ De^{-z\tau} & Ce^{-z\tau} \end{pmatrix} \\ &= \begin{pmatrix} zI & -I \\ -B - De^{-z\tau} & zI - A - Ce^{-z\tau} \end{pmatrix}. \end{aligned} \tag{2.32}$$

To compute the determinant of this block matrix, we can use Schur's formula. Since the top-right block is $-I$, which commutes with any matrix, the determinant simplifies to the product of the top-left and bottom-right blocks minus the product of the off-diagonal blocks:

$$\begin{aligned} \det \Delta_{1\mathrm{st}}(z) &= \det\Big(zI(zI - A - Ce^{-z\tau}) - (-I)(-B - De^{-z\tau})\Big) \\ &= \det\Big(z^2 I - zA - B - (zC + D)e^{-z\tau}\Big). \end{aligned} \tag{2.33}$$

What remains inside the determinant is exactly the characteristic matrix associated with our second-order equation. Therefore, we define the second-order characteristic matrix as:

$$\Delta_2(z) := z^2 I - zA - B - (zC + D)e^{-z\tau}. \tag{2.34}$$

Because $\det \Delta_{1\text{st}}(z) = \det \Delta_2(z)$, the roots of both characteristic equations are identical, preserving their algebraic and geometric multiplicities. This allows us to state the following stability results, adapted from [7] to our second-order formulation.

Lemma 2.2.1 (Distribution of Roots)**.** *The roots of the characteristic equation* $\det \Delta_2(z) = 0$ *satisfy the following properties:*

i) They are isolated, and any vertical strip in the complex plane contains only a finite number of them.

ii) There exists a real number α such that all roots are confined to the left half-plane:

$$\mathrm{Re}(z) \le \alpha.$$

iii) The roots in the left half-plane are asymptotically bounded by a curve of the form:

$$|\operatorname{Im}(z)| \le K e^{-\operatorname{Re}(z)} \quad \textit{for some } K > 0.$$

Recall from Section 2.1 that A_2 acts on pairs (ψ, v) in the Banach space $X = C^0([-\tau, 0], \mathbb{C}^n) \times \mathbb{C}^n$, defined in (2.2) and equipped with the norm $\|(\psi, v)\|_X = \|\psi\|_{C^0} + |v|$ of (2.3), as

$$A_2(\psi, v) = (\psi', \psi(-\tau)), \tag{2.35}$$

with domain

$$D(A_2) = \Big\{(\psi, v) \in C^1([-\tau, 0], \mathbb{C}^n) \times \mathbb{C}^n \;:\; \psi'(0) = A\psi(0) + B\phi(0) + C\psi(-\tau) + Dv\Big\}, \tag{2.36}$$

as in (2.17)–(2.18), where $\phi(t) = v + \int_{-\tau}^{t} \psi(\theta)\, d\theta$.

On the other hand, the augmented first-order operator acts on a pair $(u_1, u_2)^T$ as

$$A_0 \begin{pmatrix} u_1 \\ u_2 \end{pmatrix} = \begin{pmatrix} u_1' \\ u_2' \end{pmatrix}, \tag{2.37}$$

with its domain defined through the companion block matrices B_0 and B_1 (2.30):

$$D(A_0) = \left\{ \begin{pmatrix} u_1 \\ u_2 \end{pmatrix} \in C^1([-\tau, 0]; \mathbb{C}^{2n}) \;\Big|\; \begin{pmatrix} u_1 \\ u_2 \end{pmatrix}'(0) = B_0 \begin{pmatrix} u_1 \\ u_2 \end{pmatrix}(0) + B_1 \begin{pmatrix} u_1 \\ u_2 \end{pmatrix}(-\tau) \right\}. \tag{2.38}$$

The pair $(u_1, u_2)^T$ acts on the space $Y := C^0([-\tau, 0], \mathbb{C}^n) \times C^0([-\tau, 0], \mathbb{C}^n)$, which we equip with the norm $\|(\phi, \psi)\|_Y := \|\phi\|_{C^0} + \|\psi\|_{C^0}$, analogous to (2.3). A_0 is the generator of the corresponding semigroup $\{T_0(s)\}_{s\geq 0}$ on Y, defined as in Definition 2.1.1: given $(u_1, u_2) \in Y$, let $y = (y_1, y_2)$ solve (2.29) with $y|_{[-\tau,0]} = (u_1, u_2)$, and set $T_0(s)(u_1(t), u_2(t)) := \big(y_1(s+t), y_2(s+t)\big)\big|_{[-\tau,0]}$. This is the semigroup on which the method of Irastorza-Zabalegi and Ponce-Vanegas [4] is built.

Rather than comparing $D(A_2)$ and $D(A_0)$ directly, we relate X and Y through two explicit operators.

A lifting operator. Define $L : X \to Y$ by

$$L(\psi, v) := (\phi, \psi), \qquad \phi(t) = v + \int_{-\tau}^{t} \psi(\theta)\, d\theta, \tag{2.39}$$

using the same ϕ as in (2.4). We claim that L is bounded, with $\|L(\psi, v)\|_Y \leq (1+\tau)\|(\psi, v)\|_X$. In fact, for any $t \in [-\tau, 0]$, the triangle inequality gives $|\phi(t)| \leq |v| + \left|\int_{-\tau}^{t} \psi(\theta)\, d\theta\right|$, in addition:

$$\left|\int_{-\tau}^{t} \psi(\theta)\, d\theta\right| \leq \int_{-\tau}^{t} |\psi(\theta)|\, d\theta \leq (t+\tau)\|\psi\|_{C^0} \leq \tau\|\psi\|_{C^0}, \tag{2.40}$$

where the second-to-last step bounds $|\psi(\theta)| \leq \|\psi\|_{C^0}$ pointwise. Hence $|\phi(t)| \leq |v| + \tau\|\psi\|_{C^0}$ for every t, so $\|\phi\|_{C^0} \leq |v| + \tau\|\psi\|_{C^0}$, and

$$\|L(\psi, v)\|_Y = \|\phi\|_{C^0} + \|\psi\|_{C^0} \leq |v| + (1+\tau)\|\psi\|_{C^0} \leq (1+\tau)\|(\psi, v)\|_X. \tag{2.41}$$

A projection operator. Define $\Pi : Y \to X$ by

$$\Pi(\phi, \psi) := (\psi,\, \phi(-\tau)). \tag{2.42}$$

Since $-\tau \in [-\tau, 0]$, $|\phi(-\tau)| \leq \|\phi\|_{C^0}$ directly from the definition of the supremum norm, then

$$\|\Pi(\phi, \psi)\|_X = \|\psi\|_{C^0} + |\phi(-\tau)| \leq \|\psi\|_{C^0} + \|\phi\|_{C^0} = \|(\phi, \psi)\|_Y, \tag{2.43}$$

so Π is bounded with norm at most 1.

The two compositions. For $(\psi, v) \in X$, $\Pi(L(\psi, v)) = \Pi(\phi, \psi) = (\psi, \phi(-\tau)) = (\psi, v)$, since $\phi(-\tau) = v + \int_{-\tau}^{-\tau} \psi = v$. Thus

$$\Pi L = \mathrm{Id}_X. \tag{2.44}$$

In the other order, $L(\Pi(\phi, \psi)) = L(\psi, \phi(-\tau)) = (\Phi, \psi)$ with $\Phi(t) = \phi(-\tau) + \int_{-\tau}^{t} \psi(\theta)\, d\theta$, which by the Fundamental Theorem of Calculus equals ϕ if and only if $\phi' = \psi$. So $L\Pi$ recovers the identity only on pairs of the specific form (ϕ, ϕ'); it does not equal Id_Y on all of Y.

This last observation identifies the subspace on which L and Π are mutually inverse:

$$\mathcal{V} := \{(\phi, \phi') : \phi \in C^1([-\tau, 0], \mathbb{C}^n)\} \subset Y. \tag{2.45}$$

$\mathcal{V}$ is a linear subspace of Y, and it is closed: if $(\phi_k, \phi_k') \to (\phi, \psi)$ in Y, then $\phi_k \to \phi$ and $\phi_k' \to \psi$ uniformly on $[-\tau, 0]$, and since $\phi_k(t) = \phi_k(-\tau) + \int_{-\tau}^{t} \phi_k'(\theta)\, d\theta$, passing to the limit under the integral sign (justified by uniform convergence) gives $\phi(t) = \phi(-\tau) + \int_{-\tau}^{t} \psi(\theta)\, d\theta$, i.e. $\phi' = \psi$, so $(\phi, \psi) \in \mathcal{V}$. A closed subspace of a Banach space is itself a Banach space. By definition, $\mathcal{V}$ is exactly the range of L, that is $\mathcal{V} = L(X)$, and (2.44) together with $L\Pi|_{\mathcal{V}} = \mathrm{Id}_{\mathcal{V}}$ shows that

$$L : X \to \mathcal{V} \quad \text{and} \quad \Pi|_{\mathcal{V}} : \mathcal{V} \to X \tag{2.46}$$

are mutually inverse bounded linear bijections; that is, L is an isomorphism of Banach spaces between X and $\mathcal{V}$.

Invariance of $\mathcal{V}$ under T_0. For $(\phi, \phi') \in \mathcal{V}$, $T_0(s)(\phi(t), \phi'(t)) = \big(y_1(s+t),\, y_2(s+t)\big)$, where $y = (y_1, y_2)$ solves (2.29) with initial data (ϕ, ϕ'); since this initial data satisfies $y_2 = y_1'$ on $[-\tau, 0]$ and (2.29) identifies y_2 with y_1' for $t \geq 0$ as well, $y_2(s+t)$ remains the derivative of $y_1(s+t)$. Hence $T_0(s)(\phi, \phi') \in \mathcal{V}$ for every $s \geq 0$: $\mathcal{V}$ is invariant under $\{T_0(s)\}_{s \geq 0}$, and its restriction $T_0(s)|_{\mathcal{V}}$ is itself a C_0-semigroup on $\mathcal{V}$.

The identity $\Pi T_0(s) L = T_2(s)$, which relates the augmented system with the direct semi-group for the second-order DDE, can be established noticing that both sides map (ψ, v) to $(u'(s+t)|_{[-\tau,0]},\, u(s-\tau))$, where u solves (2.1). From $\Pi L = \mathrm{Id}_X$ and $L\Pi|_{\mathcal{V}} = \mathrm{Id}_{\mathcal{V}}$ we see that

$$L\, T_2(s) = T_0(s)\, L, \qquad s \geq 0. \tag{2.47}$$

Since L is an invertible, bounded linear map with bounded inverse $\Pi|_{\mathcal{V}}$, (2.47) says that T_2 and $T_0|_{\mathcal{V}}$ are similar semigroups, related by the change of representation L.

Differentiating (2.47) at $s = 0$ gives the corresponding relation between generators. For $(\psi, v) \in X$ with $L(\psi, v) \in D(A_0)$,

$$\begin{aligned} A_2(\psi, v) &= \lim_{s \to 0^+} \frac{T_2(s)(\psi, v) - (\psi, v)}{s} \\ &= \lim_{s \to 0^+} \Pi \left(\frac{T_0(s)L(\psi, v) - L(\psi, v)}{s} \right) \\ &= \Pi\big(A_0 L(\psi, v)\big), \end{aligned} \tag{2.48}$$

where the second equality uses (2.44) and the linearity of Π, and the last equality uses that Π is bounded, hence continuous, so it commutes with the limit. That is,

$$A_2 = \Pi\, A_0\, L. \tag{2.49}$$

Because $A_0(\phi, \phi') = (\phi', \phi'')$ maps $\mathcal{V} \cap D(A_0)$ back into $\mathcal{V}$, the restricted generator $A_0|_{\mathcal{V} \cap D(A_0)}$ is the generator of $T_0(s)|_{\mathcal{V}}$, and (2.49) identifies it, via the isomorphism L, with A_2. Evaluating the boundary condition of (2.38) at $L(\psi, v) = (\phi, \psi)$ gives, using $\phi' = \psi$ and $\phi(-\tau) = v$,

$$\psi'(0) = B_0 \begin{pmatrix} \phi(0) \\ \psi(0) \end{pmatrix}_2 + B_1 \begin{pmatrix} \phi(-\tau) \\ \psi(-\tau) \end{pmatrix}_2 = A\psi(0) + B\phi(0) + C\psi(-\tau) + Dv, \tag{2.50}$$

which is exactly the boundary condition of (2.36). Consequently,

$$L\big(D(A_2)\big) = D(A_0) \cap \mathcal{V}. \tag{2.51}$$

Since $D(A_0)$ imposes no relation between u_1 and u_2 away from $s = 0$, it contains pairs that do not belong to $\mathcal{V}$, so (2.51) gives the strict inclusion

$$L(D(A_2)) \subsetneq D(A_0). \tag{2.52}$$

Although $D(A_0)$ is not contained in $\mathcal{V}$, we can prove the following theorem.

Theorem 2.2.1. *All the generalized eigenfunctions of A_0 are contained in $\mathcal{V}$.*

Proof. For every $N \geq 1$, we have to prove that if $(A_0 - \lambda I)^{N-1}u \in \mathcal{D}(A_0)$ and $(A_0 - \lambda I)^N u = 0$, then $u = (u_1, u_2) \in \mathcal{V}$. In fact, we will prove by induction the stronger assertion that if $(A_0 - \lambda I)^{N-1}u \in \mathcal{D}(A_0)$ and $(A_0 - \lambda I)^N u \in \mathcal{V}$, then $u_2 = u_1'$.

For $N = 1$, solving the first-order differential equation $(A_0 - \lambda I)u = (g, g') \in \mathcal{V}$ we have that

$$\begin{pmatrix} u_1 \\ u_2 \end{pmatrix} = \begin{pmatrix} c_1 \\ c_2 \end{pmatrix} e^{\lambda t} + \int_{-\tau}^{t} e^{\lambda(t-s)} \begin{pmatrix} g \\ g' \end{pmatrix}(s)\, ds, \tag{2.53}$$

for some constant vectors $c_1, c_2 \in \mathbb{C}^n$. Since $(u_1, u_2) \in D(A_0)$, the boundary condition (2.38) must also hold; evaluating it on this candidate solution gives

$$\begin{aligned} \lambda \begin{pmatrix} c_1 \\ c_2 \end{pmatrix} + \lambda \int_{-\tau}^{0} e^{-\lambda s} \begin{pmatrix} g \\ g' \end{pmatrix}(s)\, ds + \begin{pmatrix} g \\ g' \end{pmatrix}(0) \\ = \begin{pmatrix} 0 & I \\ B & A \end{pmatrix} \left[\begin{pmatrix} c_1 \\ c_2 \end{pmatrix} + \int_{-\tau}^{0} e^{-\lambda s} \begin{pmatrix} g \\ g' \end{pmatrix}(s)\, ds \right] \\ + e^{-\lambda\tau} \begin{pmatrix} 0 & 0 \\ D & C \end{pmatrix} \begin{pmatrix} c_1 \\ c_2 \end{pmatrix}. \end{aligned} \tag{2.54}$$

The first block row of this equation gives

$$\lambda c_1 + \lambda \int_{-\tau}^{0} e^{-\lambda s} g(s)\, ds + g(0) = c_2 + \int_{-\tau}^{0} e^{-\lambda s} g'(s)\, ds \tag{2.55}$$

Comparing with (2.53), we see that $u_2 = u_1'$ on $[-\tau, 0]$, so $(u_1, u_2) \in \mathcal{V}$.

Now, let us assume that the claim holds for all $k < N$. Then, writing $(A_0 - \lambda I)^{N-1}(A_0 - \lambda I)u \in \mathcal{V}$, we see by the induction hypothesis that $(A_0 - \lambda I)u \in \mathcal{V}$. Since $u \in \mathcal{D}(A_0)$, then applying the case $N = 1$ we conclude that $u \in \mathcal{V}$, as we wanted to prove. □

Consequently, the point spectrum of A_0 coincides with that of $A_0|_{\mathcal{V}}$: every eigenvalue of one is an eigenvalue of the other, with the same eigenvectors. Both operators can therefore be used to compute the eigenvalues of the second-order delay differential equation, but $A_0|_{\mathcal{V}}$ — equivalently, A_2, through the isomorphism L of (2.46) — involves fewer degrees of freedom once discretized.

2.3 Stability

To analyze the asymptotic behavior and stability of the C_0-semigroup $\{T_2(s)\}_{s\geq 0}$ generated by A_2, we can rely on the established theory for first-order DDEs [7]. Since A_2 is a representation of $A_0|_{\mathcal{V}}$, and all the generalized eigenfunctions are contained in $\mathcal{V}$, then most of the results in [7] carry over to A_2.

Theorem 2.3.1 (Asymptotic Expansion)**.** *Let $u(t)$ be a solution to the second-order DDE. For any real number $\gamma \in \mathbb{R}$, the solution can be expressed as a finite sum of exponential terms corresponding to the characteristic roots plus a faster-decaying remainder:*

$$u(t) = \sum_{\mathrm{Re}(\lambda_j)\geq\gamma} p_j(t)e^{\lambda_j t} + o\left(e^{\gamma t}\right) \quad \text{as } t \to \infty, \tag{2.56}$$

where λ_j are the roots of $\det \Delta_2(z) = 0$, and each $p_j(t)$ is a $\mathbb{C}^n$-valued polynomial given by:

$$p_j(t) = \sum_{k=0}^{m_j-1} t^k c_{j,k}, \tag{2.57}$$

with m_j representing the algebraic multiplicity of the eigenvalue λ_j and $c_{j,k} \in \mathbb{C}^n$.

The terms in the expansion are generalized eigenfunctions. This expansion immediately yields the following criterion for exponential stability.

Corollary 2.3.1 (Exponential Stability)**.** *All solutions of the system converge exponentially to zero as $t \to \infty$ if and only if $\det \Delta_2(z) = 0$ has no roots in the closed right half-plane $\{\mathrm{Re}(z) \geq 0\}$.*

Consequently, assessing the stability of the infinite-dimensional system is reduced to locating the roots of the scalar equation $\det \Delta_2(z) = 0$ in the complex plane. The final piece of the theoretical framework connects these roots directly to the spectrum of our generator A_2.

Theorem 2.3.2 (Spectrum of the Generator)**.** *The spectrum of the infinitesimal generator A_2 is given purely by its point spectrum, which corresponds to the roots of the characteristic equation:*

$$\sigma(A_2) = \{\lambda \in \mathbb{C} : \det \Delta_2(\lambda) = 0\}. \tag{2.58}$$

Moreover, the geometric multiplicity of an eigenvalue λ coincides with $\dim\ker \Delta_2(\lambda)$, and its algebraic multiplicity corresponds to the order of λ as a zero of the analytic function $\det \Delta_2(z)$.

While a fully rigorous mathematical proof of this theorem relies on demonstrating that A_2 has a compact resolvent operator [7], we can intuitively motivate this theorem algebraically.

We seek an eigenvalue $\lambda \in \mathbb{C}$ and a non-zero eigenfunction pair $(\psi, v) \in D(A_2)$ such that $A_2(\psi, v) = \lambda(\psi, v)$. Let us look for a pair corresponding to an exponential solution $u(t) = ce^{\lambda t}$ with $c \in \mathbb{C}^n \backslash \{0\}$. Its derivative and its delayed value at $t = -\tau$ are given by:

$$\psi(\theta) = \lambda c e^{\lambda\theta} \quad (\theta \in [-\tau, 0]), \qquad v = ce^{-\lambda\tau}. \tag{2.59}$$

By definition of the operator $A_2(\psi, v) = (\psi', \psi(-\tau))$, this pair automatically satisfies $\psi'(\theta) = \lambda^2 c e^{\lambda\theta} = \lambda\psi(\theta)$ and $\psi(-\tau) = \lambda c e^{-\lambda\tau} = \lambda v$.

The non-trivial restriction arises from requiring that (ψ, v) belongs to the domain $D(A_2)$. We first evaluate $\phi(0)$:

$$\begin{aligned}\phi(0) &= v + \int_{-\tau}^{0} \psi(\theta)\, d\theta = ce^{-\lambda\tau} + \int_{-\tau}^{0} \lambda c e^{\lambda\theta}\, d\theta \\ &= ce^{-\lambda\tau} + \Big[ce^{\lambda\theta}\Big]_{-\tau}^{0} = ce^{-\lambda\tau} + c - ce^{-\lambda\tau} = c. \end{aligned} \tag{2.60}$$

Now, we impose the domain boundary condition $\psi'(0) = A\psi(0) + B\phi(0) + C\psi(-\tau) + Dv$. Substituting $\psi'(0) = \lambda^2 c$, $\psi(0) = \lambda c$, $\phi(0) = c$, $\psi(-\tau) = \lambda c e^{-\lambda\tau}$, and $v = ce^{-\lambda\tau}$, we obtain:

$$\lambda^2 c = A(\lambda c) + Bc + C(\lambda c e^{-\lambda\tau}) + D(ce^{-\lambda\tau}), \tag{2.61}$$

which reorganizes directly into:

$$\left[\lambda^2 I - \lambda A - B - (\lambda C + D)e^{-\lambda\tau}\right]c = 0. \tag{2.62}$$

This is exactly $\Delta_2(\lambda)c = 0$. Since c must be non-zero for the eigenfunction to be non-trivial, the matrix $\Delta_2(\lambda)$ must be singular, meaning $\det \Delta_2(\lambda) = 0$. This illustrates why the eigenvalues of the abstract infinite-dimensional generator are precisely the roots of the concretely computable matrix $\Delta_2(\lambda)$.

In summary, the asymptotic behavior and stability of the second-order delay differential equation are governed by the location of its characteristic roots. Specifically, all solutions of the system converge exponentially to zero as $t \to \infty$ if and only if the characteristic equation has no roots in the closed right half-plane:

$$\det \Delta_2(\lambda) = 0 \quad \text{for all } \lambda \in \mathbb{C} \text{ with } \operatorname{Re}(\lambda) \geq 0. \tag{2.63}$$

Equivalently, this stability criterion can be stated in terms of the operator theory developed herein; the system is exponentially stable if and only if the entire spectrum of the infinitesimal generator A_2 lies strictly within the open left half-plane:

$$\sigma(A_2) \subset \{\lambda \in \mathbb{C} : \operatorname{Re}(\lambda) < 0\}. \tag{2.64}$$

This result reduces an abstract, infinite-dimensional stability problem into a concrete and computationally checkable algebraic condition, setting the foundation for the numerical analysis that follows.

2.4 The Cayley Transform Approach

Since the infinitesimal generator A_2 is an unbounded operator, developing stable and efficient numerical methods directly from its definition presents mathematical and computational challenges. To overcome this difficulty, we adopt the framework proposed by Irastorza-Zabalegi and Ponce-Vanegas [4], which utilizes a functional calculus approach to map the unbounded operator into a bounded one. While classical approaches, such as the semi-discretization method, rely on the exponential map $\varphi_h(z) = e^{hz}$, the exponential mapping is not one-to-one due to its periodicity in the complex plane. Instead, we employ the Cayley transform, also referred to in numerical contexts as the Tustin method or bilinear transform [4]. The primary advantage of this transformation is that it is a one-to-one mapping, ensuring that the spectral properties and eigenvalues can be faithfully and uniquely recovered.

For a complex variable $z \in \mathbb{C}$, the Cayley transform $\varphi_C(z)$ is defined by setting the parameters to their natural choice $a = b = 1$:

$$\varphi_C(z) = \frac{1+z}{1-z}, \quad z \neq 1. \tag{2.65}$$

Geometrically, this specific configuration maps the open left half-plane, which represents the region of asymptotic stability for our continuous system, directly into the interior of the open unit disk:

$$\mathcal{H} := \{z \in \mathbb{C} : \mathrm{Re}(z) < 0\} \xrightarrow{\varphi_C} \mathbb{D} := \{w \in \mathbb{C} : |w| < 1\}. \tag{2.66}$$

To lift this transformation to the operator level, we assume that $1 \notin \sigma(A_2)$. Since the spectrum of A_2 is discrete and purely pointwise, this assumption is mild and can be satisfied for a generic system. The transformed operator $\varphi_C(A_2)$ is defined as:

$$\varphi_C(A_2) = (I + A_2)(I - A_2)^{-1}. \tag{2.67}$$

By exploiting the algebraic properties of the resolvent operator and evaluating the general transform identity at $a = b = 1$, we establish the following relation for any $\lambda \in \mathbb{C} \setminus \{1\}$:

$$\varphi_C(A_2) - \varphi_C(\lambda)I = \frac{2}{1-\lambda}(A_2 - \lambda I)(I - A_2)^{-1}. \tag{2.68}$$

Equation (2.68) serves as the bridge connecting the original eigenvalue problem of A_2 with that of the bounded operator $\varphi_C(A_2)$. This algebraic relationship leads directly to the spectral mapping theorem for the Cayley transform.

Lemma 2.4.1 (Spectral Mapping under Cayley Transform [4])**.** *Let A_2 be the infinitesimal generator and assume $1 \notin \sigma(A_2)$. Then, the spectrum of the transformed operator satisfies:*

$$\sigma(\varphi_C(A_2)) \setminus \{-1\} = \varphi_C(\sigma(A_2)). \tag{2.69}$$

Furthermore, since the delay differential equation possesses infinitely many characteristic roots, the point -1 is an accumulation point of the transformed eigenvalues and satisfies $-1 \in \sigma(\varphi_C(A_2))$.

Proof. The first assertion follows immediately from the identity (2.68) and the fact that $-1 \notin \varphi_C(\mathbb{C})$. For the second part, because the system has infinitely many characteristic roots, their magnitudes are unbounded in the left half-plane. Thus, there exists a sequence of eigenvalues $\{\lambda_i\}_{i=1}^{\infty} \subset \sigma(A_2)$ such that $|\lambda_i| \to \infty$ as $i \to \infty$. Applying the transform yields:

$$\lim_{i\to\infty} \varphi_C(\lambda_i) = \lim_{i\to\infty} \frac{1+\lambda_i}{1-\lambda_i} = -1. \tag{2.70}$$

Since the spectrum of any closed operator is a closed set in the complex plane, the limit point must belong to the spectrum, concluding that $-1 \in \sigma(\varphi_C(A_2))$. $\square$

2.4.1 Action of the Transformed Operator $\mathcal{T}$

To implement the Cayley transform numerically, we must determine the explicit action of the bounded operator $\mathcal{T} := \varphi_C(A_2)$ on an arbitrary element (ψ, v) of the space X. By definition, the transformed operator evaluated at $a = b = 1$ is given by:

$$\mathcal{T}(\psi, v) = (I + A_2)(I - A_2)^{-1}(\psi, v). \tag{2.71}$$

The evaluation is split into two steps. First, we must compute the resolvent action, defining $(f, g) := (I - A_2)^{-1}(\psi, v)$. This is equivalent to solving the operator equation:

$$(f, g) - A_2(f, g) = (\psi, v). \tag{2.72}$$

Recalling the action of the infinitesimal generator $A_2(f, g) = (f', f(-\tau))$, the system (2.72) decomposes into a functional equation and a vector equation:

$$f(\theta) - f'(\theta) = \psi(\theta), \quad \theta \in [-\tau, 0], \tag{2.73}$$
$$g - f(-\tau) = v. \tag{2.74}$$

We solve the first-order ordinary differential equation (2.73) by applying the change of variables $f(\theta) = p(\theta)e^{\theta}$. Differentiating this expression yields $f'(\theta) = p'(\theta)e^{\theta} + p(\theta)e^{\theta}$. Substituting these into the differential equation, the terms $p(\theta)e^{\theta}$ cancel out, leaving:

$$-p'(\theta)e^{\theta} = \psi(\theta) \implies p'(\theta) = -e^{-\theta}\psi(\theta). \tag{2.75}$$

Integrating from the delayed boundary $-\tau$ to an arbitrary $\theta \in [-\tau, 0]$, we obtain:

$$p(\theta) - p(-\tau) = -\int_{-\tau}^{\theta} e^{-s}\psi(s)\, ds. \tag{2.76}$$

Let us define the integration constant $K := p(-\tau) \in \mathbb{C}^n$. The parameter $p(\theta)$ is then given by:

$$p(\theta) = K - \int_{-\tau}^{\theta} e^{-s}\psi(s)\, ds. \tag{2.77}$$

Multiplying back by e^{θ}, we obtain the exact expression for the functional component $f(\theta)$:

$$f(\theta) = Ke^{\theta} - \int_{-\tau}^{\theta} e^{\theta-s}\psi(s)\, ds. \tag{2.78}$$

Evaluating this solution at the boundaries of the delay interval yields:

$$f(-\tau) = Ke^{-\tau}, \tag{2.79}$$

$$f(0) = K - \int_{-\tau}^{0} e^{-s}\psi(s)\,ds. \tag{2.80}$$

To ensure that the resulting pair (f, g) belongs to the domain $D(A_2)$, it must satisfy the boundary condition of the original system. Let $\eta : [-\tau, 0] \to \mathbb{C}^n$ be the state history function associated with (f, g), defined analogously to the initial condition function ϕ of the original equation:

$$\eta(t) = g + \int_{-\tau}^{t} f(s)\,ds. \tag{2.81}$$

We evaluate this function at $t = 0$ to apply the domain condition. By substituting $f(s) = f'(s) + \psi(s)$ from (2.73) directly into the integral, we obtain a algebraic simplification:

$$\eta(0) = g + \int_{-\tau}^{0} (f'(s) + \psi(s))\,ds = g + f(0) - f(-\tau) + \int_{-\tau}^{0} \psi(s)\,ds. \tag{2.82}$$

From the vector equation (2.74), we know that $g = v + f(-\tau)$. Substituting g into $\eta(0)$ exactly cancels the $f(-\tau)$ terms:

$$\eta(0) = v + f(0) + \int_{-\tau}^{0} \psi(s)\,ds. \tag{2.83}$$

Inserting the expression for $f(0)$ from (2.80), the function $\eta(0)$ simplifies exclusively in terms of K and the known data (ψ, v):

$$\eta(0) = v + K - \int_{-\tau}^{0} e^{-s}\psi(s)\,ds + \int_{-\tau}^{0} \psi(s)\,ds. \tag{2.84}$$

The domain condition requires that the pair (f, g) satisfies the underlying differential equation at $\theta = 0$:

$$f'(0) = Af(0) + B\eta(0) + Cf(-\tau) + Dg. \tag{2.85}$$

From the ordinary differential equation, $f'(0) = f(0) - \psi(0)$. Replacing the left-hand side of (2.85) and substituting equations (2.74), (2.79), (2.80), and (2.84), we formulate the full equality:

$$\begin{aligned}\left(K - \int_{-\tau}^{0} e^{-s}\psi(s)\,ds\right) - \psi(0) = A&\left(K - \int_{-\tau}^{0} e^{-s}\psi(s)\,ds\right)\\ &+ B\left(v + K - \int_{-\tau}^{0} e^{-s}\psi(s)\,ds + \int_{-\tau}^{0} \psi(s)\,ds\right)\\ &+ C\left(Ke^{-\tau}\right) + D\left(v + Ke^{-\tau}\right). \end{aligned} \tag{2.86}$$

We gather all terms multiplying the constant K on the left side of the equation:

$$\left(I - A - B - (C + D)e^{-\tau}\right) K = \dots \tag{2.87}$$

We immediately recognize the matrix multiplying K as the characteristic matrix evaluated at 1, namely $\Delta_2(1)$. Moving the remaining integrals and constant terms to the right side and grouping them produces:

$$\Delta_2(1)K = (I - A - B)\int_{-\tau}^{0} e^{-s}\psi(s)\,ds + (B + D)v + \psi(0) + B\int_{-\tau}^{0} \psi(s)\,ds. \tag{2.88}$$

Assuming $1 \notin \sigma(A_2)$, the matrix $\Delta_2(1)$ is invertible, which uniquely determines the constant K:

$$K = \Delta_2(1)^{-1}\left[(I - A - B)\int_{-\tau}^{0} e^{-s}\psi(s)\,ds + (B + D)v + \psi(0) + B\int_{-\tau}^{0} \psi(s)\,ds\right]. \tag{2.89}$$

Finally, with the resolvent action determined, we apply the forward mapping $(I + A_2)$ to the pair (f, g) to obtain the output of the transformed operator:

$$\mathcal{T}(\psi, v) = (I + A_2)(f, g) = \big(f(\theta) + f'(\theta),\ g + f(-\tau)\big). \tag{2.90}$$

Using the relations $f'(\theta) = f(\theta) - \psi(\theta)$ and $g = v + f(-\tau)$, we simplify the components to their final computational form:

$$\mathcal{T}(\psi, v) = \big(2f(\theta) - \psi(\theta),\ v + 2Ke^{-\tau}\big), \tag{2.91}$$

To better highlight the underlying algebraic structure of the Cayley transform, we can substitute the explicit form of $f(\theta)$ given in (2.78) back into the expression of the transformed operator. By factoring out the state pair $-(\psi, v)$, we isolate the identity operator and express $\mathcal{T}(\psi, v)$ in a form that reflects the classical abstract operator identity $\mathcal{T} = -I + 2(I - A_2)^{-1}$:

$$\mathcal{T}(\psi, v) = -(\psi, v) + 2\left(Ke^{\theta} - \int_{-\tau}^{\theta} e^{\theta - s}\psi(s)\,ds,\ v + Ke^{-\tau}\right). \tag{2.92}$$

At this stage, note that the integration constant $K \in \mathbb{C}^n$ is a linear vector function that depends uniquely and explicitly on the choice of the input data pair. To emphasize this functional dependence throughout the formulation, we shall henceforth denote it explicitly as $K(\psi, v)$.

Following the framework established by Irastorza-Zabalegi and Ponce-Vanegas, we introduce a slight modification to the Cayley transform operator by employing a similarity transformation via an exponential scaling. Setting the weight parameter to $b = 1$, we define the scaling operator $E_1 : X \to X$ and its inverse $E_{-1} : X \to X$ as:

$$E_1(\psi, v) = (e^{\theta}\psi, v), \quad \text{and} \quad E_{-1}(\psi, v) = (e^{-\theta}\psi, v). \tag{2.93}$$

The modified Tustin operator $T : X \to X$ is then defined by the composition:

$$T(\psi, v) := E_{-1}\mathcal{T}E_1(\psi, v). \tag{2.94}$$

We evaluate this modified action step by step. First, applying the forward scaling maps the arbitrary initial state pair (ψ, v) to the weighted data pair $(e^{\theta}\psi, v)$. Consequently, when the original transform $\mathcal{T}$ acts upon these modified data, the internal integration constant is evaluated at these scaled arguments, becoming $K(e^\theta\psi, v)$. Substituting these into the operator yields:

$$\begin{aligned}\mathcal{T}(e^\theta\psi, v) = -(e^\theta\psi, v) + 2\Big(&K(e^\theta\psi, v)e^\theta - \int_{-\tau}^{\theta} e^{\theta-s}\left(e^s\psi(s)\right)\, ds,\\ &v + K(e^\theta\psi, v)e^{-\tau}\Big).\end{aligned} \tag{2.95}$$

Notice that the integrand in the functional component simplifies directly since $e^{\theta-s}e^s = e^\theta$. This allows the exponential term to be factored out of the integral:

$$K(e^\theta\psi, v)e^\theta - \int_{-\tau}^{\theta} e^\theta\psi(s)\, ds = e^\theta\Big(K(e^\theta\psi, v) - \int_{-\tau}^{\theta}\psi(s)\, ds\Big). \tag{2.96}$$

Finally, we apply the inverse scaling operator E_{-1}, which multiplies the functional component by $e^{-\theta}$ while leaving the vector component unaltered (as $e^{-1\cdot 0} = 1$). This leads to a remarkable algebraic cancellation where the exponential factors disappear entirely from the functional block. Regrouping the terms, we arrive at the final clean expression for the modified operator:

$$T(\psi, v) = -(\psi, v) + 2\left(K(e^\theta\psi, v) - \int_{-\tau}^{\theta}\psi(s)\, ds,\ K(e^\theta\psi, v)e^{-\tau} + v\right). \tag{2.97}$$

This formulation is advantageous for numerical implementations, as it isolates the trivial identity mapping, avoiding any numerical stiffness associated with the exponential weights inside the state evaluation.

Next, we show that this modification preserves the eigenvalues of the original operator $\mathcal{T}$ unaltered, as it constitutes a similarity transformation. Assume that λ is an eigenvalue of $\mathcal{T}$ with an associated non-zero eigenpair $(\psi, v) \in X$, meaning that:

$$\mathcal{T}(\psi, v) = \lambda(\psi, v). \tag{2.98}$$

By defining a new transformed eigenpair as $(\tilde{\psi}, \tilde{v}) := E_{-1}(\psi, v)$, and utilizing the identity property $E_1E_{-1} = I$, we apply the modified operator $T = E_{-1}\mathcal{T}E_1$ to this element:

$$\begin{aligned}T(\tilde{\psi}, \tilde{v}) &= (E_{-1}\mathcal{T}E_1)\,(E_{-1}(\psi, v))\\ &= E_{-1}\mathcal{T}(E_1E_{-1})(\psi, v)\\ &= E_{-1}\mathcal{T}(\psi, v).\end{aligned} \tag{2.99}$$

Substituting the original eigenvalue relation $\mathcal{T}(\psi, v) = \lambda(\psi, v)$ and exploiting the linearity of the scaling operator E_{-1}, we directly obtain:

$$\begin{aligned}T(\tilde{\psi}, \tilde{v}) &= E_{-1}\big(\lambda(\psi, v)\big)\\ &= \lambda E_{-1}(\psi, v)\\ &= \lambda(\tilde{\psi}, \tilde{v}).\end{aligned} \tag{2.100}$$

This demonstrates that λ is also an eigenvalue of the modified operator T under the transformed eigenpair $(\tilde{\psi}, \tilde{v})$, guaranteeing that the stability and the spectrum of the original system remain unaltered.

2.5 Discretization using Linear Splines

To compute the eigenvalues of the modified operator T numerically, we must project the infinite-dimensional problem onto a finite-dimensional subspace. This is achieved through a sequence of projections P_M such that the finite-dimensional approximations approach the true operator as the dimension M increases. To build a numerical scheme, we adapt the Galerkin framework proposed by Irastorza-Zabalegi and Ponce-Vanegas [4] to our product space $X = C([-\tau, 0]; \mathbb{C}^n) \times \mathbb{C}^n$.

2.5.1 The Functional Basis and Collocation Projection

To discretize the bounded operator T over our specific space $X = C([-\tau, 0]; \mathbb{C}^n) \times \mathbb{C}^n$, our initial approach relies on constructing a sequence of projections P_M into finite-dimensional subspaces U_M. We discretize only the first component because the second one is already finite-dimensional. We define a uniform mesh over the delay interval $[-\tau, 0]$ consisting of M nodes (including the boundaries), which gives a step size of $h = \tau/(M-1)$. The nodal points are thus given by $s_k = -\tau + (k-1)h$ for $k = 1, \dots, M$.

To approximate the infinite-dimensional functional component of our space, we utilize linear B-splines (degree $d = 1$), denoted as $\{\varphi_k\}_{k=1}^M$. Because our system is n-dimensional, a natural basis for the functional subspace is given by the tensor product $\{\varphi_k \otimes \mathbf{e}_j\}$, where $k = 1, \dots, M$ and $\mathbf{e}_j$ represents the canonical basis vectors of $\mathbb{C}^n$.

A dual basis of $\{\varphi_k \otimes \mathbf{e}_j\}$, is $\{\varphi^k \otimes \mathbf{e}^j\}$, where $\{\varphi^k\}_{k=1}^M$ are the Borel measures $\varphi^k = \delta_{s_k}$, and δ_{s_k} is the Dirac delta at $s_k \in [-\tau, 0]$. This dual basis acts on a vector-valued function ψ via $(\varphi^k \otimes \mathbf{e}_j)\psi = \mathbf{e}_j^T \psi(s_k)$, which allows us to "read" each individual scalar component of the continuous function at the mesh points.

Using this framework, we can define the mappings that bridge the continuous space and the discrete computational space. First, we define the finite-dimensional space $X_M := \mathbb{C}^{Mn} \times \mathbb{C}^n$. We then introduce the projection operator $\pi_h : X \to X_M$, which compresses a continuous state pair by evaluating the function component by component at the nodes using the dual basis, while leaving the vector component unchanged:

$$\pi_h(\psi, v) = \Big((\varphi^1 \otimes \mathbf{e}^1)\psi,\, \dots,\, (\varphi^1 \otimes \mathbf{e}^n)\psi,\, \dots,\, (\varphi^M \otimes \mathbf{e}^1)\psi,\, \dots,\, (\varphi^M \otimes \mathbf{e}^n)\psi,\, v\Big). \tag{2.101}$$

Conversely, we define the inclusion operator $\iota_h : X_M \to X$, which reconstructs a continuous state pair from a discrete vector of coordinates $Z = (z_{1,1}, \dots, z_{1,n}, \dots, z_{M,1}, \dots, z_{M,n}) \in \mathbb{C}^{Mn}$ and $v \in \mathbb{C}^n$:

$$\iota_h(Z, v) = \left(\sum_{k=1}^{M} \sum_{j=1}^{n} z_{k,j}(\varphi_k \otimes \mathbf{e}_j),\, v\right). \tag{2.102}$$

By composing these two mappings, we construct the total orthogonal projection $P_M := \iota_h \pi_h$. Consequently, the infinite-dimensional modified operator T can be approximated in the computer by its finite matrix representation:

$$T_M := \pi_h T \iota_h. \tag{2.103}$$

These would be the elements of the matrix related to the first component:

$$(T_M)_{(n,i),(m,j)} = (\delta_{s_n} \otimes \mathbf{e}^i)\big(T_M(\varphi_m \otimes \mathbf{e}_j)\big) \tag{2.104}$$

2.5.2 Transition to the Sobolev Space H^1

To gain access to a broader set of functional techniques (such as the Galerkin method), we replace the space of continuous functions with the Hilbert space $H^1([-\tau, 0]; \mathbb{C}^n)$. Consequently, our working space becomes:

$$X_{H^1} := H^1([-\tau, 0]; \mathbb{C}^n) \times \mathbb{C}^n. \tag{2.105}$$

Operating in this space preserves all the essential spectral properties of the system, as summarized in the following properties.

Lemma 2.5.1 (Properties of the Operator in H^1 [4])**.** *The modified operator T acting on the space X_{H^1} satisfies the following:*

i) T is a well-defined and bounded operator in X_{H^1}.

ii) It can be decomposed as $T = -I + K$, where K is a compact operator.

iii) The generalized eigenfunctions of T are sufficiently smooth to belong to H^1. Therefore, the spectrum remains invariant: $\sigma(T|_{X_{H^1}}) = \sigma(T)$.

The proof of this result relies on the compactness of the integral operator through the Rellich–Kondrachov embedding theorem. For a rigorous mathematical demonstration of these properties, the reader is referred to [4] and the functional analysis literature cited therein.

2.5.3 Subspace Decomposition and Sparse Matrices

We strategically choose a basis that neutralizes the dense nature of the integral terms. We split the functional space $H^1([-\tau, 0]; \mathbb{C}^n)$ into a direct sum $H_0 \oplus H_0^{\perp}$, where H_0 is defined as the subspace of functions that vanish at the boundaries and with vanishing mean:

$$H_0 := \left\{ \psi \in H^1([-\tau, 0]; \mathbb{C}^n) : \psi(-\tau) = \psi(0) = 0 \text{ and } \int_{-\tau}^{0} \psi(s)\, ds = 0 \right\}. \tag{2.106}$$

This decomposition underlies the computational efficiency of the method. When evaluating the action of the operator $T(\psi, v)$ on a state pair where the functional component belongs to H_0, the definite integral over the delay interval strictly vanishes. This mathematically isolates the non-local operations to the small complementary subspace $H_0^{\perp}$. As a result, the vast majority of the operator's action becomes purely local, guaranteeing that the resulting discretized matrices are sparse.

To explicitly construct the basis for this complementary subspace $H_0^\perp$, we utilize the standard inner product in $H^1([-\tau,0];\mathbb{C}^n)$:

$$\langle \phi, \psi \rangle_{H^1} = \int_{-\tau}^{0} \left(\phi(s)\overline{\psi(s)} + \phi'(s)\overline{\psi'(s)} \right) ds. \tag{2.107}$$

By definition, any function $\phi \in H_0^\perp$ must satisfy $\langle \phi, \psi \rangle_{H^1} = 0$ for all $\psi \in H_0$. Applying integration by parts to the derivative term, we get:

$$\int_{-\tau}^{0} \phi'(s)\overline{\psi'(s)}\, ds = \left[\phi(s)\overline{\psi(s)} \right]_{-\tau}^{0} - \int_{-\tau}^{0} \phi''(s)\overline{\psi(s)}\, ds. \tag{2.108}$$

Since $\psi \in H_0$, the boundary conditions $\psi(-\tau) = \psi(0) = 0$ eliminate the boundary terms. The orthogonality condition then simplifies to:

$$\int_{-\tau}^{0} \left(\phi(s) - \phi''(s) \right) \overline{\psi(s)}\, ds = 0. \tag{2.109}$$

Because this integral must vanish for all functions ψ that have a zero net integral ($\int_{-\tau}^{0} \psi(s) ds = 0$), the term in parentheses must be equal to a constant. Thus, the functions in $H_0^\perp$ must satisfy the second-order linear differential equation:

$$\phi''(s) - \phi(s) = -C, \quad C \in \mathbb{C}. \tag{2.110}$$

The general solution to this non-homogeneous second-order differential equation can be expressed as the sum of a particular constant solution and the general solution to the homogeneous equation $\phi''(s) - \phi(s) = 0$. This yields a 3-dimensional functional subspace. To preserve symmetry over the generic interval $[-\tau, 0]$, we shift the coordinate center to the midpoint $-\tau/2$. This allows us to define a natural spanning set for $H_0^\perp$ composed of a constant, a hyperbolic sine, and a hyperbolic cosine:

$$\mathcal{B} = \left\{ 1,\ \sinh\left(s + \frac{\tau}{2}\right),\ \cosh\left(s + \frac{\tau}{2}\right) \right\}. \tag{2.111}$$

To construct a mutually orthogonal basis $\{\tilde{\phi}_1, \tilde{\phi}_2, \tilde{\phi}_3\}$ from this set under the H^1 inner product, we proceed step by step:

1. **First basis function:** We choose the constant function as our starting element:

$$\tilde{\phi}_1(s) = 1. \tag{2.112}$$

Its squared H^1-norm is easily computed as:

$$\langle 1, 1 \rangle_{H^1} = \int_{-\tau}^{0} \left(1 \cdot 1 + 0 \cdot 0 \right) ds = \tau. \tag{2.113}$$

2. **Second basis function:** We test the hyperbolic sine function, $\psi_2(s) = \sinh\left(s + \frac{\tau}{2}\right)$. Computing its inner product with $\tilde{\phi}_1$ yields:

$$\begin{aligned} \langle \tilde{\phi}_1, \psi_2 \rangle_{H^1} &= \int_{-\tau}^{0} \left(1 \cdot \sinh\left(s + \frac{\tau}{2}\right) + 0 \cdot \cosh\left(s + \frac{\tau}{2}\right) \right) ds \\ &= \left[\cosh\left(s + \frac{\tau}{2}\right) \right]_{-\tau}^{0} = \cosh\left(\frac{\tau}{2}\right) - \cosh\left(-\frac{\tau}{2}\right). \end{aligned} \tag{2.114}$$

Since $\cosh(x)$ is an even function, $\cosh(-\tau/2) = \cosh(\tau/2)$, meaning the integral vanishes ($\langle \tilde{\phi}_1, \psi_2 \rangle_{H^1} = 0$). Thus, they are already orthogonal due to symmetry, and we can directly set:

$$\tilde{\phi}_2(s) = \sinh\left(s + \frac{\tau}{2}\right). \tag{2.115}$$

3. **Third basis function:** We consider the hyperbolic cosine function, $\psi_3(s) = \cosh\left(s + \frac{\tau}{2}\right)$. First, its inner product with $\tilde{\phi}_2$ vanishes because the resulting integrand contains products of even and odd functions symmetric about the midpoint $-\tau/2$:

$$\begin{aligned}\langle \tilde{\phi}_2, \psi_3 \rangle_{H^1} = \int_{-\tau}^{0} \Bigg(&\sinh\left(s + \frac{\tau}{2}\right)\cosh\left(s + \frac{\tau}{2}\right) \\ &+ \cosh\left(s + \frac{\tau}{2}\right)\sinh\left(s + \frac{\tau}{2}\right)\Bigg) ds = 0.\end{aligned} \tag{2.116}$$

However, computing its inner product with the constant function $\tilde{\phi}_1$ reveals that they are not orthogonal:

$$\begin{aligned}\langle \tilde{\phi}_1, \psi_3 \rangle_{H^1} &= \int_{-\tau}^{0} \left(1 \cdot \cosh\left(s + \frac{\tau}{2}\right) + 0 \cdot \sinh\left(s + \frac{\tau}{2}\right)\right) ds \\ &= \left[\sinh\left(s + \frac{\tau}{2}\right)\right]_{-\tau}^{0} = 2\sinh\left(\frac{\tau}{2}\right).\end{aligned} \tag{2.117}$$

To fix this, we apply the Gram-Schmidt process and subtract the projection of ψ_3 onto $\tilde{\phi}_1$:

$$\tilde{\phi}_3(s) = \psi_3(s) - \frac{\langle \tilde{\phi}_1, \psi_3 \rangle_{H^1}}{\langle \tilde{\phi}_1, \tilde{\phi}_1 \rangle_{H^1}} \tilde{\phi}_1(s) = \cosh\left(s + \frac{\tau}{2}\right) - \frac{2\sinh\left(\frac{\tau}{2}\right)}{\tau} \cdot 1. \tag{2.118}$$

This systematic orthogonalization yields the final set of unnormalized orthogonal basis functions:

$$\tilde{\phi}_1(s) = 1, \tag{2.119}$$

$$\tilde{\phi}_2(s) = \sinh\left(s + \frac{\tau}{2}\right), \tag{2.120}$$

$$\tilde{\phi}_3(s) = \cosh\left(s + \frac{\tau}{2}\right) - \frac{2}{\tau}\sinh\left(\frac{\tau}{2}\right). \tag{2.121}$$

The final orthonormal basis functions $\{\phi_1, \phi_2, \phi_3\}$ are obtained simply by dividing each $\tilde{\phi}_k(s)$ by its respective H^1-norm, yielding the analytical functions used to discretize the non-local part of the delay operator.

2.5.4 Galerkin Projection and Block Matrix Structure

To construct the finite-dimensional subspaces $U_M \subset X_{H^1}$, we discretize the delay interval $[-\tau, 0]$ using a uniform mesh of M nodes, with a step size of $h = \tau/(M-1)$. The functional approximation space is built by combining the specialized basis for

H_0, constructed by taking the difference of two consecutive linear B-splines to guarantee a zero net integral, and the orthonormal analytical basis derived for $H_0^{\perp}$. Let $\{\psi_m\}_{m=1}^{M_{\text{func}}}$ denote this combined scalar functional basis.

Our system evolves in the product space $X_{H^1} = H^1([-\tau, 0]; \mathbb{C}^n) \times \mathbb{C}^n$, meaning a state consists of a historical functional component and a current finite-dimensional vector component. Therefore, the complete basis for the discrete subspace U_M must independently span both components. We construct the total basis $\mathcal{B}_{U_M}$ by taking the union of two distinct sets of elements:

$$\mathcal{B}_{U_M} = \Big\{ \big(\psi_m \otimes \mathbf{e}_i,\, \mathbf{0}\big) \Big\} \bigcup \Big\{ \big(\mathbf{0},\, \mathbf{e}_i\big) \Big\}, \tag{2.122}$$

where $m = 1, \ldots, M_{\text{func}}$ and $i = 1, \ldots, n$. The first set purely spans the functional history, while the second set spans the instantaneous vector state at $s = 0$.

To perform the Galerkin projection, we define the total inner product on the product space X_{H^1} as the sum of the standard inner products of its constituent spaces:

$$\big\langle (\phi, u),\, (\psi, v) \big\rangle_{X_{H^1}} = \langle \phi, \psi \rangle_{H^1} + \langle u, v \rangle_{\mathbb{C}^n}. \tag{2.123}$$

This explicit separation of the basis elements imposes a rigorous four-block structure on the resulting matrices. The Galerkin projection $P_M T P_M$ translates the continuous operator into a generalized eigenvalue problem:

$$\mathbf{A}\mathbf{v} = \mu \mathbf{B}\mathbf{v}. \tag{2.124}$$

The mass matrix $\mathbf{B}$ captures the non-orthogonality of the basis elements and is constructed using the total inner product $\langle \Psi_k, \Psi_l \rangle_{X_{H^1}}$. Thanks to the separated basis, $\mathbf{B}$ inherently takes the form:

$$\mathbf{B} = \begin{pmatrix} \mathbf{B}_{11} & \mathbf{B}_{12} \\ \mathbf{B}_{21} & \mathbf{B}_{22} \end{pmatrix} = \begin{pmatrix} \langle \psi_m \otimes \mathbf{e}_i,\, \psi_k \otimes \mathbf{e}_j \rangle_{H^1} & \mathbf{0} \\ \mathbf{0} & \mathbf{I}_n \end{pmatrix}. \tag{2.125}$$

Notice that the cross-blocks $\mathbf{B}_{12}$ and $\mathbf{B}_{21}$ vanish identically because the functional and vector basis components do not overlap (one has a zero vector, the other has a zero function). Furthermore, the bottom-right block $\mathbf{B}_{22}$ simplifies to the exact identity matrix $\mathbf{I}_n$ since $\langle (\mathbf{0}, \mathbf{e}_i), (\mathbf{0}, \mathbf{e}_j) \rangle_{X_{H^1}} = \langle \mathbf{e}_i, \mathbf{e}_j \rangle_{\mathbb{C}^n} = \delta_{ij}$.

Similarly, the stiffness matrix $\mathbf{A}$, whose entries are formed by $\langle T(\Psi_k), \Psi_l \rangle_{X_{H^1}}$, exhibits a complementary 4-block structure:

$$\mathbf{A} = \begin{pmatrix} \mathbf{A}_{11} & \mathbf{A}_{12} \\ \mathbf{A}_{21} & \mathbf{A}_{22} \end{pmatrix}. \tag{2.126}$$

Unlike the mass matrix, the cross-blocks $\mathbf{A}_{12}$ and $\mathbf{A}_{21}$ are generally dense and non-zero, as the action of the delay operator T intrinsically couples the historical state with the current dynamics.

Solving this block-structured generalized eigenvalue problem yields the numerical approximations μ for the spectrum of the modified operator T. Finally, using the inverse Cayley mapping, we recover the dominant roots of the original infinitesimal generator A_2, characterizing the stability of the delay differential equation.

2.6 Time-Scaling and Delay Normalization

From a computational perspective, fixing the delay parameter to a unitary value ($\tau = 1$) simplifies both the mesh generation and the numerical evaluation of the analytical basis functions. This choice does not restrict the generality of the method, as any linear second-order delay differential equation with an arbitrary delay $\tau > 0$ can be mapped to a normalized system with a delay of 1 via a time-scaling transformation.

Consider our original second-order delay differential equation:

$$u''(t) = Au'(t) + Bu(t) + Cu'(t-\tau) + Du(t-\tau). \tag{2.127}$$

We introduce the dimensionless time variable $\hat{t} := t/\tau$. Defining the scaled state variable as $\hat{u}(\hat{t}) := u(\tau\hat{t}) = u(t)$, we can express the time derivatives using the chain rule:

$$u'(t) = \frac{d}{dt}u(t) = \frac{1}{\tau}\frac{d}{d\hat{t}}\hat{u}(\hat{t}) = \frac{1}{\tau}\hat{u}'(\hat{t}), \tag{2.128}$$

$$u''(t) = \frac{d^2}{dt^2}u(t) = \frac{1}{\tau^2}\frac{d^2}{d\hat{t}^2}\hat{u}(\hat{t}) = \frac{1}{\tau^2}\hat{u}''(\hat{t}). \tag{2.129}$$

For the delayed terms, the time shift transforms as $u(t-\tau) = \hat{u}\left(\frac{t-\tau}{\tau}\right) = \hat{u}(\hat{t}-1)$, meaning the physical delay τ is mapped to a normalized delay of 1.

Substituting these scaled derivatives and delayed states into the original differential equation yields:

$$\frac{1}{\tau^2}\hat{u}''(\hat{t}) = A\left(\frac{1}{\tau}\hat{u}'(\hat{t})\right) + B\hat{u}(\hat{t}) + C\left(\frac{1}{\tau}\hat{u}'(\hat{t}-1)\right) + D\hat{u}(\hat{t}-1). \tag{2.130}$$

To isolate the highest-order derivative, we multiply the entire equation by τ^2, arriving at the normalized system:

$$\hat{u}''(\hat{t}) = (\tau A)\hat{u}'(\hat{t}) + (\tau^2 B)\hat{u}(\hat{t}) + (\tau C)\hat{u}'(\hat{t}-1) + (\tau^2 D)\hat{u}(\hat{t}-1). \tag{2.131}$$

This mathematical equivalence guarantees that analyzing the stability of a second-order system with an arbitrary delay τ is identical to analyzing a transformed system operating over a normalized delay interval $[-1, 0]$. Consequently, the numerical framework implemented for $\tau = 1$ preserves complete mathematical generality: it can be applied to any system by simply scaling the damping matrices (A, C) by τ and the stiffness matrices (B, D) by τ^2 prior to assembling the discretized operators.

Based on this equivalence, the computational code developed for this thesis has been structurally optimized and implemented assuming a fixed normalized delay of $\tau = 1$. By hardcoding this unitary value, the numerical engine avoids the algorithmic overhead associated with dynamic mesh resizing and the repetitive re-evaluation of the spline basis functions for different delays. Consequently, all numerical simulations, validation benchmarks, and case studies presented throughout the remainder of this work are executed using this fixed-delay configuration.

For practical engineering applications operating under an arbitrary physical delay, the stability analysis can be conducted without modifying the code. The normalization is handled entirely during the preprocessing stage by adjusting the input matrices according to the derived scaling rules; specifically, mapping $A \to \tau A$, $B \to \tau^2 B$, $C \to \tau C$, and $D \to \tau^2 D$.

Chapter 3

Case Study and Simulations

The code implementing the algorithm developed in this thesis is available at `https://gitlab.bcamath.org/auyarra/ddemultiple`; further details are provided in the README.

3.1 Numerical Validation of the Cayley Transform

To numerically validate the Galerkin discretization scheme and the spectral mapping properties of the Cayley transform, we construct a test case using a new set of randomly generated complex, dense matrices. This configuration ensures that the dynamical system possesses no trivial symmetries or uncoupled dynamics that could artificially mask numerical inaccuracies. We parameterize our second-order delay differential equation with the following matrices:

$$A = \begin{pmatrix} 0.2654 + 0.8004i & -0.9523 - 0.6753i \\ 2.6169 + 2.5129i & 0.3900 - 1.4639i \end{pmatrix}, \tag{3.1}$$

$$B = \begin{pmatrix} 1.3205 - 1.6092i & -0.7017 - 0.4254i \\ -1.8789 - 0.6783i & -0.9787 + 0.6243i \end{pmatrix}, \tag{3.2}$$

$$C = \begin{pmatrix} 1.1303 - 1.0798i & -0.2948 + 1.4163i \\ -0.0518 + 1.6844i & 0.5782 + 0.4072i \end{pmatrix}, \tag{3.3}$$

$$D = \begin{pmatrix} 4.7894 - 0.4644i & 1.8349 - 1.0035i \\ -0.2245 + 2.2576i & -0.7244 - 1.3956i \end{pmatrix}. \tag{3.4}$$

Figure 3.1 and Figure 3.2 visualize the computed spectrum of this test system. The numerical results illustrate the topological changes introduced by the Cayley mapping. In the original domain (right side of the figures), the stability boundary is strictly defined by the imaginary axis ($\Re(\lambda) = 0$). The transformed domain (left side of the figures) wraps this boundary directly onto the unit circle ($|\mu| = 1$).

Two theoretical properties of delay differential equations and the Cayley transform are visually confirmed in these results:

1. **Mapping of Unstable Roots:** The tested system exhibits exactly five unstable eigenvalues. In the original continuous spectrum, these five roots possess a strictly positive real part ($\Re(\lambda) > 0$). Accordingly, the Cayley transform correctly projects these specific five eigenvalues to the exterior of the unit circle in the discrete complex plane ($|\mu| > 1$).

2. **Collapse of the Infinite Spectrum:** Delay differential equations are characterized by an infinite number of highly damped eigenvalues that extend deeply into the stable left half-plane ($\Re(\lambda) \to -\infty$). Under the Cayley transform, this infinite asymptotic tail is mathematically compacted. As distinctly observed in the numerical spectrum, all these highly stable roots converge and densely accumulate precisely at the point -1 on the real axis of the transformed plane.

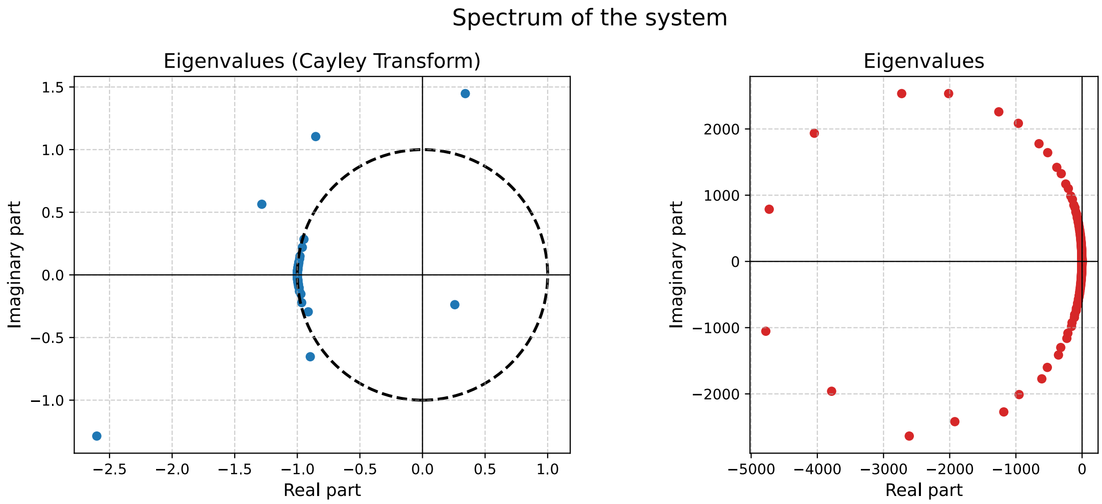

Figure 3.1: General view of the computed spectrum. Left: Discrete eigenvalues μ mapped by the Cayley transform (stability bounded by the unit circle). Right: Continuous eigenvalues λ recovered via the inverse Cayley transform (stability bounded by the imaginary axis).

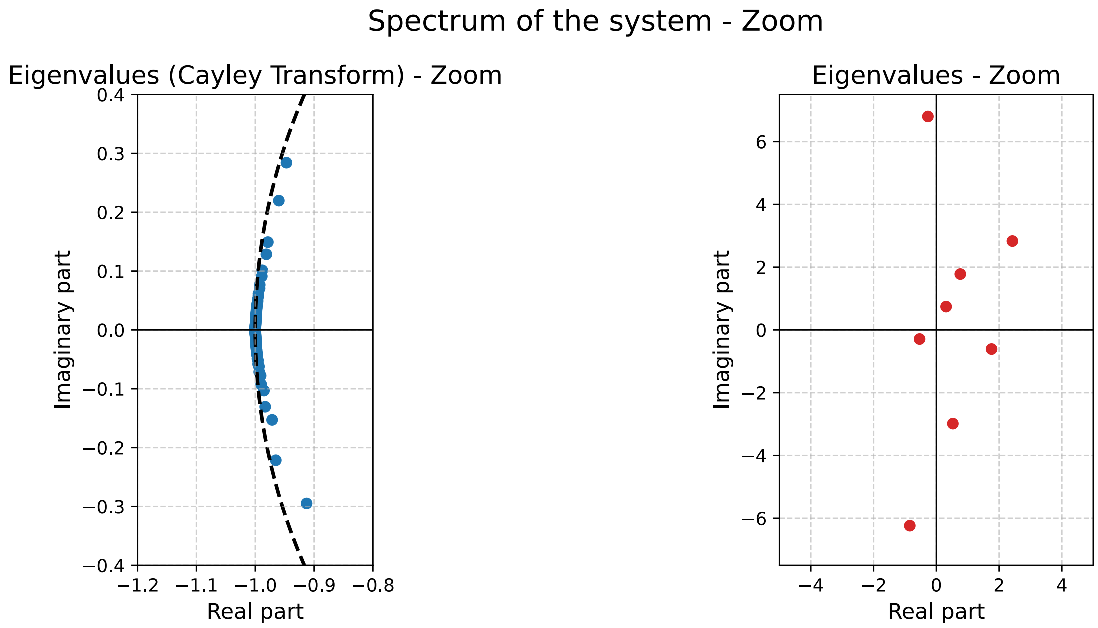

Figure 3.2: Detailed zoomed view of the spectrum. The plots highlight the structural mapping of the five unstable roots (crossing the boundaries) and the dense accumulation of the highly stable infinite spectrum at -1 in the Cayley domain.

3.2 Convergence Analysis and Spectral Resolution Limitations

To evaluate the numerical performance and convergence behavior of the proposed Galerkin projection, we analyze the behavior of the computed spectrum as a function of the number of linear B-spline elements, denoted by M. Figures 3.3a, 3.3b, 3.3c, and 3.3d depict the computed continuous eigenvalues λ for varying mesh sizes. The numerical experiments reveal a clear contrast in convergence rates: the dominant roots located near the imaginary axis ($\Re(\lambda) \approx 0$) converge rapidly with small values of M, whereas eigenvalues situated deep within the stable left half-plane ($\Re(\lambda) \to -\infty$) exhibit poor convergence and systematic deviations from their true locations, even as the mesh is refined.

This phenomenon is governed by two distinct physical and mathematical limitations:

1. **Functional Approximation and Steep Gradients:** The eigenfunctions associated with the infinitesimal generator for a given eigenvalue λ are inherently characterized by exponential profiles of the form $e^{\lambda s}$ for $s \in [-\tau, 0]$. For highly stable eigenvalues where $\Re(\lambda)$ is a large negative value, this functional component represents a sharp exponential decay with a large, localized gradient near the boundaries of the delay interval. Linear B-splines (degree $d = 1$) possess piecewise constant derivatives (straight lines) and are structurally ill-suited to capture such sharp exponential curvatures and

steep slopes. Consequently, the discrete subspace lacks the spatial resolution necessary to reconstruct these localized boundary-layer dynamics unless the element size $h = 1/(M+1)$ approaches zero aggressively.

2. **Geometric Sensitivity of the Inverse Mapping:** This functional resolution bottleneck is compounded by the geometry of the spectral transformation. The inverse Cayley transform mapping the discrete eigenvalues μ back to the continuous domain λ is explicitly defined as:

$$\lambda = f(\mu) = \frac{\mu - 1}{\mu + 1}. \tag{3.5}$$

   Evaluating the first derivative of this rational mapping yields the sensitivity operator:

$$\frac{d\lambda}{d\mu} = \frac{2}{(\mu+1)^2}. \tag{3.6}$$

   As established, the infinite sequence of highly stable roots asymptotically collapses toward the accumulation point $\mu \to -1$ in the discrete plane. In this neighborhood, the denominator of the derivative vanishes, causing the sensitivity to blow up toward infinity ($\frac{d\lambda}{d\mu} \to \infty$). Geometrically, this implies that the inverse transformation acts as an error amplifier. Any minute numerical perturbation, rounding error, or discretization inaccuracy in computing μ near the accumulation point is magnified exponentially when projected back onto the continuous λ-plane.

From an engineering and practical stability perspective, this localized lack of convergence does not compromise the utility of the method. In the context of system stability—such as the prediction of regenerative chatter—the asymptotic behavior is exclusively dictated by the rightmost, dominant eigenvalues. Since the proposed framework converges rapidly and accurately in the vicinity of the stability boundary ($\Re(\lambda) = 0$), the slow convergence of the highly damped, deep-left roots can be safely disregarded.

3.3 Influence of the System Dimension on the Spectrum

To further analyze the robustness of the numerical scheme and observe the structural behavior of the spectrum, we investigate how the dimension of the space, denoted by n, influences the distribution of the eigenvalues. For this experiment, the number of functional splines is kept constant at $M = 100$. The parameter matrices $A, B, C, D \in \mathbb{C}^{n\times n}$ are constructed as dense, random complex matrices. To prevent any unintended symmetries, both the real and imaginary parts of every matrix entry are independently drawn from a Gaussian distribution with a mean of zero ($\mu = 0$) and a standard deviation of two ($\sigma = 2$).

Figure 3.4 and Figure 3.5 illustrate the computed spectra for system dimensions $n \in \{1, 2, 3, 4\}$. The numerical results expose a clear geometric pattern in

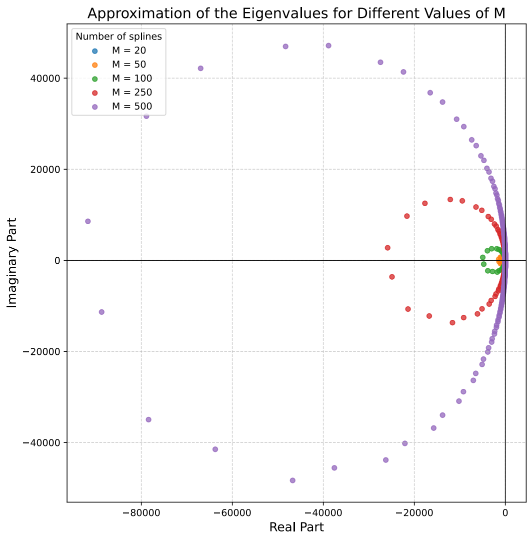

(a) Global overview of the full spectrum.

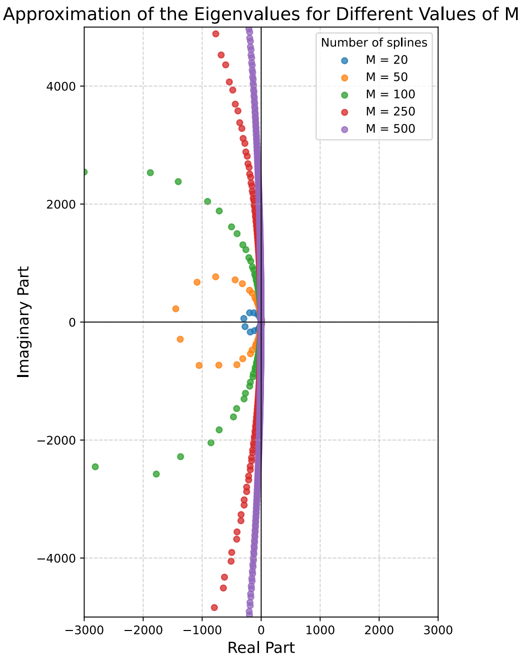

(b) Zoom 1: $\Re(\lambda) \in [-3000, 3000]$, $\Im(\lambda) \in [-5000, 5000]$.

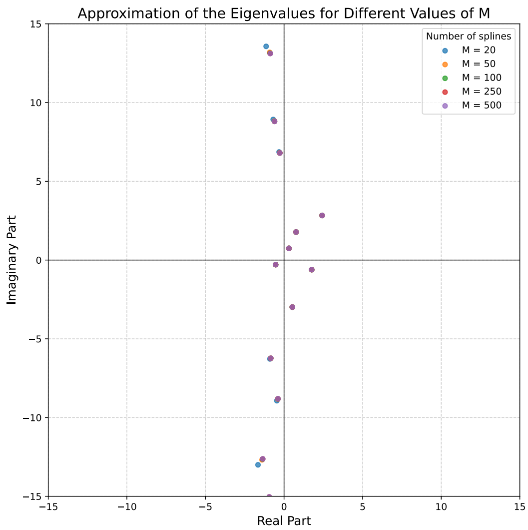

(c) Zoom 2: $\Re(\lambda) \in [-15, 15]$, $\Im(\lambda) \in [-15, 15]$.

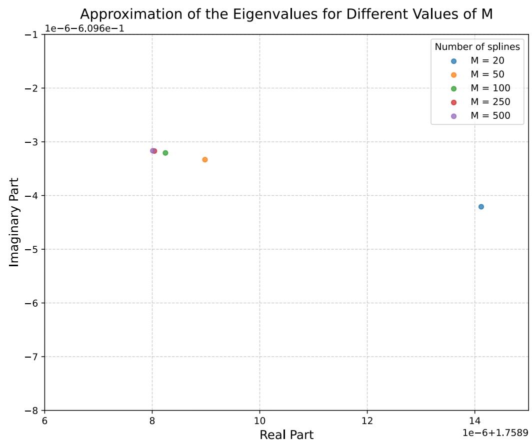

(d) Zoom 3: Micro-scale around an unstable root (10^{-6} resolution).

Figure 3.3: Continuous eigenvalue convergence analysis for different values of the mesh parameter M. (a) Global overview of the computed spectrum; (b) close-up view showing how the distinct numerical approximations closely coincide near the imaginary axis and especially in the vicinity of the origin; (c) detailed view around the origin demonstrating that the computed eigenvalues from all approximations lie directly on top of each other (completely superimposed); (d) microscopic zoom showing that a high-resolution scale of 10^{-6} is strictly required to begin visually differentiating the separate approximations of an eigenvalue with a positive real part.

the asymptotic distribution of the highly stable roots. As the eigenvalues extend deeper into the left half-plane, they organize themselves into distinct characteristic branches or asymptotic chains.

Visually, the number of these asymptotic chains correlates directly with the dimension of the system. For a scalar equation ($n = 1$), the eigenvalues follow a single continuous curve. When the dimension is increased to $n = 2$, the spectrum splits, and the roots appear in interlaced pairs. This behavior scales proportionally: a 3-dimensional system yields roots grouped in clusters of three, and a 4-dimensional system produces groupings of four distinct branches.

A rigorous theoretical analysis to formally explain why the characteristic roots of multi-dimensional delay differential equations arrange themselves into these specific n-branched asymptotic chains is beyond the scope of this work. However, this geometric spectral clustering represents a recognized phenomenon in the stability analysis of complex delayed systems. Similar asymptotic branching patterns and structural root distributions have been observed and analyzed in systems subject to large delays. To gain a deeper understanding of how these topological structures emerge within the spectrum of delay differential equations, the reader is referred to the foundational study by Lichtner, Wolfrum, and Yanchuk [6].

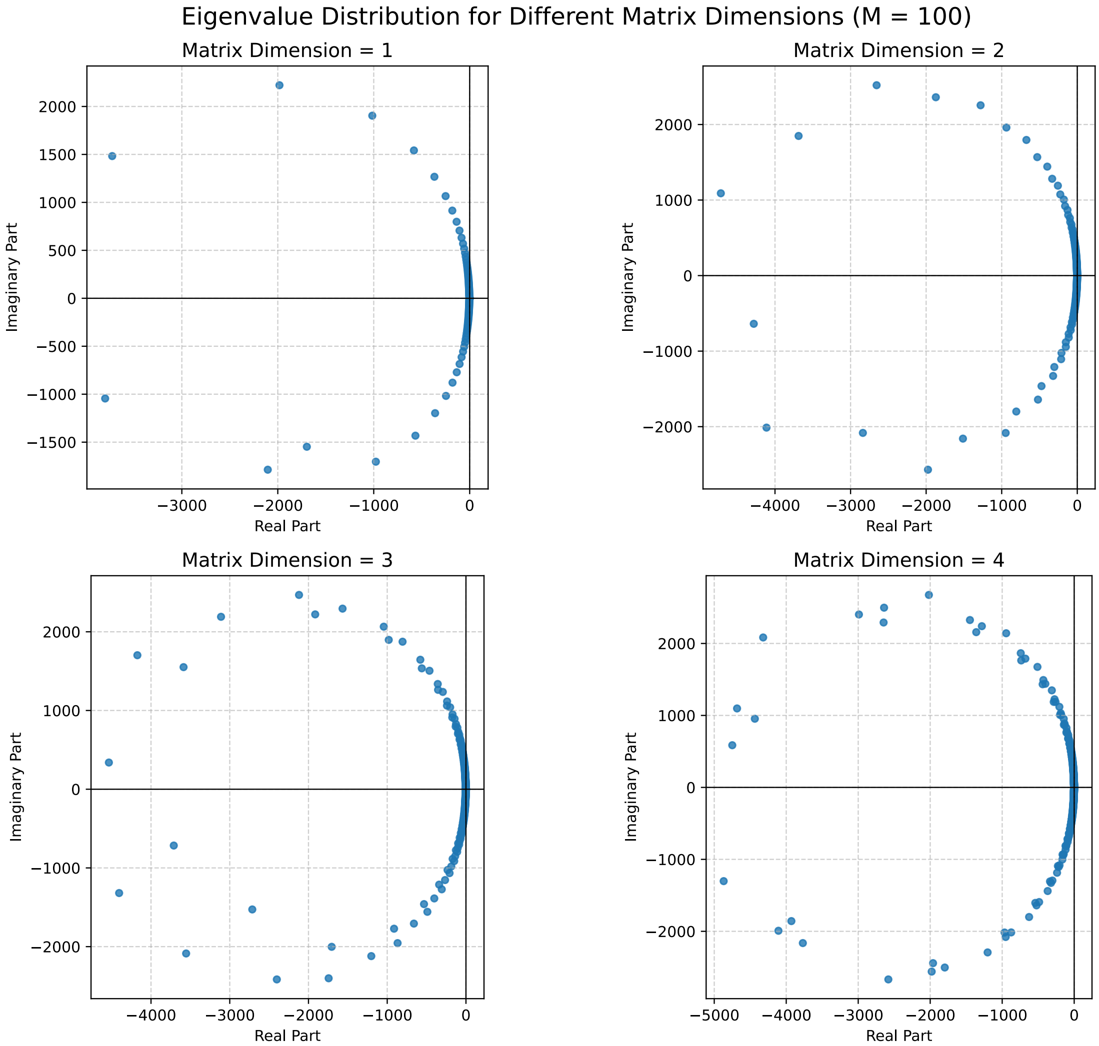

Figure 3.4: Global overview of the eigenvalue distribution for different matrix dimensions $n \in \{1, 2, 3, 4\}$. The plots clearly show the roots grouping into n distinct asymptotic branches as they extend into the stable left half-plane.

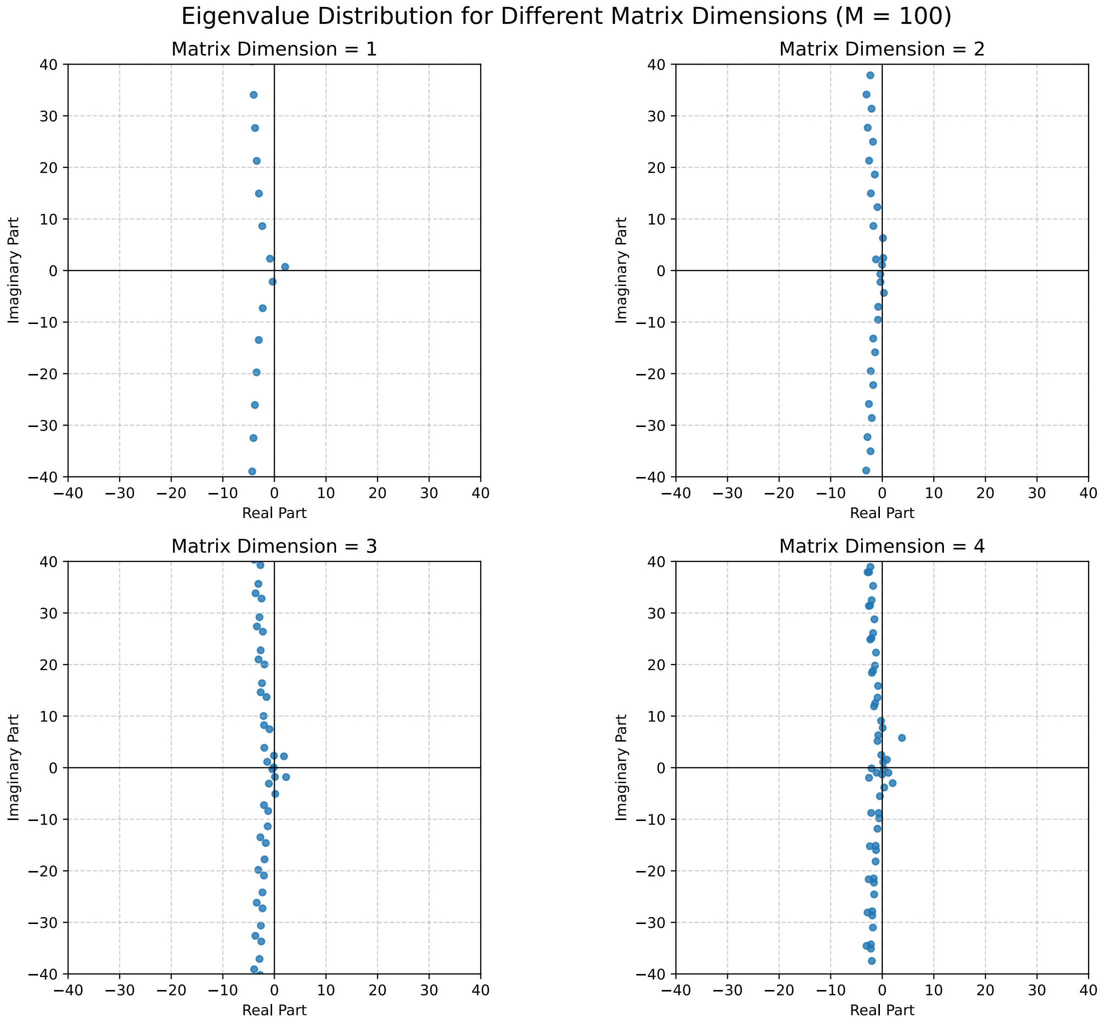

Figure 3.5: Detailed zoomed view of the spectrum near the imaginary axis for system dimensions $n \in \{1, 2, 3, 4\}$. The localized clustering of the eigenvalues according to the system dimension n is clearly observable.

3.4 A Posteriori Error Estimation and Convergence Rates

To evaluate the accuracy of the computed spectrum without prior knowledge of the exact roots, we construct a local a posteriori error estimator.

Let λ^* denote an exact root of the characteristic equation, satisfying $\det \Delta(\lambda^*) = 0$. Let $\tilde{\lambda}$ represent the numerical approximation obtained via the Galerkin projection for a given mesh size. Assuming the numerical scheme has converged sufficiently close to the exact solution, the distance $h_e = \lambda^* - \tilde{\lambda}$ is small. We can approximate the first derivative of the characteristic determinant at $\tilde{\lambda}$ using a first-order Taylor expansion (or the limit definition of the derivative prior to taking the limit):

$$(\det \Delta)'(\tilde{\lambda}) \approx \frac{\det \Delta(\lambda^*) - \det \Delta(\tilde{\lambda})}{\lambda^* - \tilde{\lambda}}. \tag{3.7}$$

By utilizing the identity $\det \Delta(\lambda^*) = 0$, the expression simplifies to:

$$(\det \Delta)'(\tilde{\lambda}) \approx \frac{0 - \det \Delta(\tilde{\lambda})}{\lambda^* - \tilde{\lambda}} = \frac{-\det \Delta(\tilde{\lambda})}{\lambda^* - \tilde{\lambda}}. \tag{3.8}$$

Rearranging this formulation allows us to isolate the approximation error. Taking the absolute value yields the a posteriori error estimator:

$$\text{error} = |\lambda^* - \tilde{\lambda}| \approx \left| \frac{\det \Delta(\tilde{\lambda})}{(\det \Delta)'(\tilde{\lambda})} \right|. \tag{3.9}$$

This index effectively scales the residual of the characteristic equation by its local sensitivity, providing a reliable measure of numerical accuracy at each individual root.

We apply this estimator to analyze the convergence behavior of the seven eigenvalues closest to the origin as a function of the element mesh size $h = 1/(M+1)$. Figure 3.6 illustrates the evolution of the logarithm of the error against $-\log(h)$ on a log-log scale for the following target roots:

$$\lambda_1 = -0.53 - 0.29i, \qquad \lambda_2 = 0.31 + 0.74i, \qquad \lambda_3 = 1.76 - 0.61i,$$
$$\lambda_4 = 0.76 + 1.78i, \qquad \lambda_5 = 0.53 - 2.99i, \qquad \lambda_6 = 2.42 + 2.83i,$$
$$\lambda_7 = -0.84 - 6.23i.$$

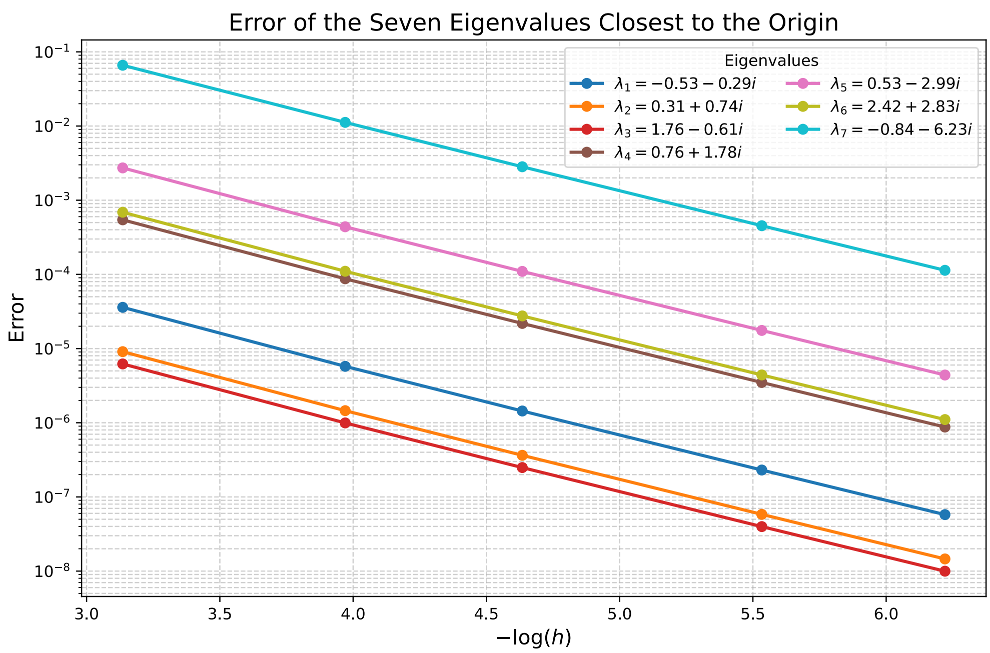

Figure 3.6: A posteriori error estimation for the seven eigenvalues closest to the origin as a function of the negative logarithm of the element size, $-\log(h)$. The linear trends reflect a steady algebraic convergence rate, with roots closer to the origin exhibiting systematically lower error magnitudes.

Two primary numerical conclusions can be drawn from these convergence curves:

1. **Algebraic Power-Law Decay:** The strictly linear decay observed for all tracking lines on the log-log scale confirms that the approximation error follows an algebraic convergence relationship of the form Error $\propto h^p$. The uniform slopes indicate a consistent and stable convergence order across the evaluated spectral region.

2. **Spatial Dependence:** The absolute magnitude of the error depends on the spatial frequency of the corresponding mode. Eigenvalues positioned closest to the origin (such as λ_1 and λ_2) exhibit lower errors compared to those located further away (such as λ_7). Physically, roots near the origin correspond to low-frequency dynamical modes whose eigenfunctions are smooth and possess minimal oscillation. Consequently, the linear B-spline subspace can approximate these shapes with high precision, whereas higher-frequency modes require a denser mesh to resolve their faster spatial variations.

3.5 Comparative Analysis with the Augmented First-Order Approach

As established in the theoretical formulation, the second-order delay differential equation can be formally rewritten as the $2n$-dimensional first-order system presented in (2.29), whose block matrices B_0 and B_1 are defined in (2.30). This classical reformulation allows the system to be solved using existing first-order numerical algorithms, such as the Cayley-based method developed by Irastorza-Zabalegi and Ponce-Vanegas. Because our proposed numerical framework operates directly on the second-order structure—avoiding the duplication of the system's dimension—it was intuitively hypothesized that our direct projection using linear B-splines ($p = 1$) would natively outperform the augmented first-order implementation using the same polynomial degree. To test this hypothesis, we compare the a posteriori error of our direct second-order method against the augmented first-order method. Figure 3.7 displays the convergence curves for two dominant eigenvalues, $\lambda_1 = -0.53 - 0.29i$ and $\lambda_2 = 0.31 + 0.74i$.

The numerical results reveal three structural conclusions:

1. **Equivalence of Linear Schemes ($p = 1$):** Contrary to our initial hypothesis, the direct second-order approach and the augmented first-order approach (both employing $p = 1$) yield practically identical convergence rates and equivalent orders of magnitude in accuracy. The marginal differences do not follow a discernible geometric or physical pattern; our method performs slightly better for λ_1, whereas the augmented method is slightly more accurate for λ_2. Extensive testing with varying system matrices confirms that this behavior is purely case-dependent, establishing numerical equivalence between both linear approaches.

2. **Higher-Order Interpolation ($p = 2$):** The first-order reference algorithm includes the computational flexibility to increase the spline degree. As mathematically expected, employing quadratic B-splines ($p = 2$) yields a much steeper convergence slope, achieving lower residual errors for the same mesh size compared to the linear models.

3. **Machine Precision Floor:** For the $p = 2$ discretization, the error decay conspicuously stalls and begins to diverge slightly as $-\log(h)$ approaches 6. This saturation does not imply algorithmic failure, but rather marks the absolute machine precision floor inherent to standard double-precision floating-point arithmetic (Float64). At error scales near 10^{-11}, evaluating the determinant residual suffers from catastrophic cancellation and numerical noise, effectively masking any further theoretical convergence.

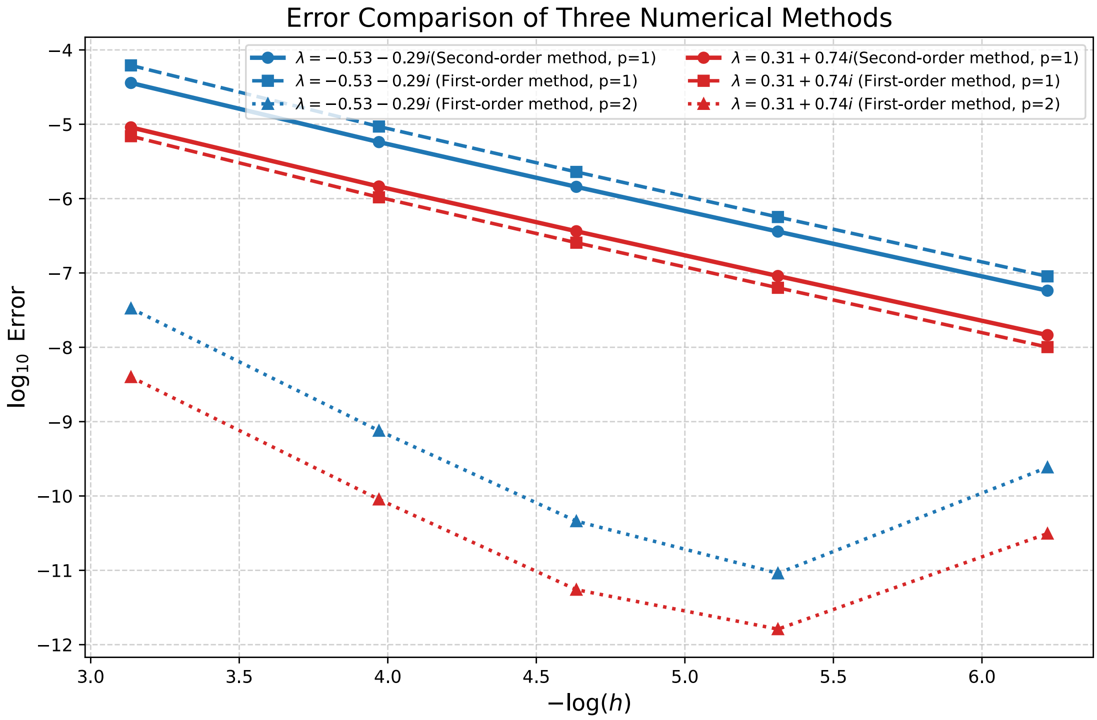

Figure 3.7: Comparison of the a posteriori error between the proposed direct second-order method (New) and the augmented first-order Tustin method utilizing linear ($p = 1$) and quadratic ($p = 2$) B-splines. The analysis demonstrates the baseline numerical equivalence of the $p = 1$ schemes and highlights the machine precision limits encountered by the $p = 2$ formulation.

3.6 Computational Efficiency and Structural Non-Redundancy

Section 3.5 showed that the direct and augmented formulations converge at the same rate for linear splines. Their computational cost is not the same, however: as shown by the strict domain inclusion (2.52), the augmented formulation carries functional degrees of freedom that the direct method does not need. This is reflected in the dimension of the resulting discrete systems, for our direct second-order method, the discretization utilizes the coupled basis:

$$\mathcal{B}_{U_M} = \Big\{ \big(\psi_m \otimes \mathbf{e}_i,\, \mathbf{0}\big) \Big\} \bigcup \Big\{ \big(\mathbf{0},\, \mathbf{e}_i\big) \Big\}, \tag{3.10}$$

where $m = 1, \ldots, M+3$ spans the B-splines and the orthogonal complement, and $i = 1, \ldots, n$ spans the physical dimension. Accounting for the $(M+3)n$ functional degrees of freedom and the n additional boundary vectors, the exact dimension of the direct matrix is $N_{\text{Direct}} = (M+4)n$. Conversely, the augmented first-order method dispenses with the independent boundary vector part but projects the $M+3$ functional elements directly onto the $2n$-dimensional augmented space, yielding an exact matrix dimension of $N_{\text{Augmented}} = 2(M+3)n$.

Standard generalized eigenvalue solvers for dense matrices, such as the QZ algorithm implemented in underlying computing libraries, exhibit a total cubic computational complexity of $\mathcal{O}(N^3)$ operations [1]. As the number of splines M increases to achieve high-fidelity refinements, the asymptotic ratio between the dimensions of both discrete systems satisfies:

$$\lim_{M\to\infty} \frac{N_{\text{Augmented}}}{N_{\text{Direct}}} = \lim_{M\to\infty} \frac{2(M+3)n}{(M+4)n} = 2. \tag{3.11}$$

Invoking the cubic scaling law of the solver, the ratio of the global computational cost asymptotically approaches:

$$\frac{\text{Cost}_{\text{Augmented}}}{\text{Cost}_{\text{Direct}}} \approx \left(\frac{N_{\text{Augmented}}}{N_{\text{Direct}}} \right)^3 \to 2^3 = 8. \tag{3.12}$$

Thus, simply by eliminating the redundant kinematic state variables, the direct second-order formulation guarantees a theoretical eightfold reduction in computational effort in the asymptotic limit. This cubic $\mathcal{O}(N^3)$ penalty explains the rapid, non-linear growth of the execution time for the augmented method observed in Figure 3.8.

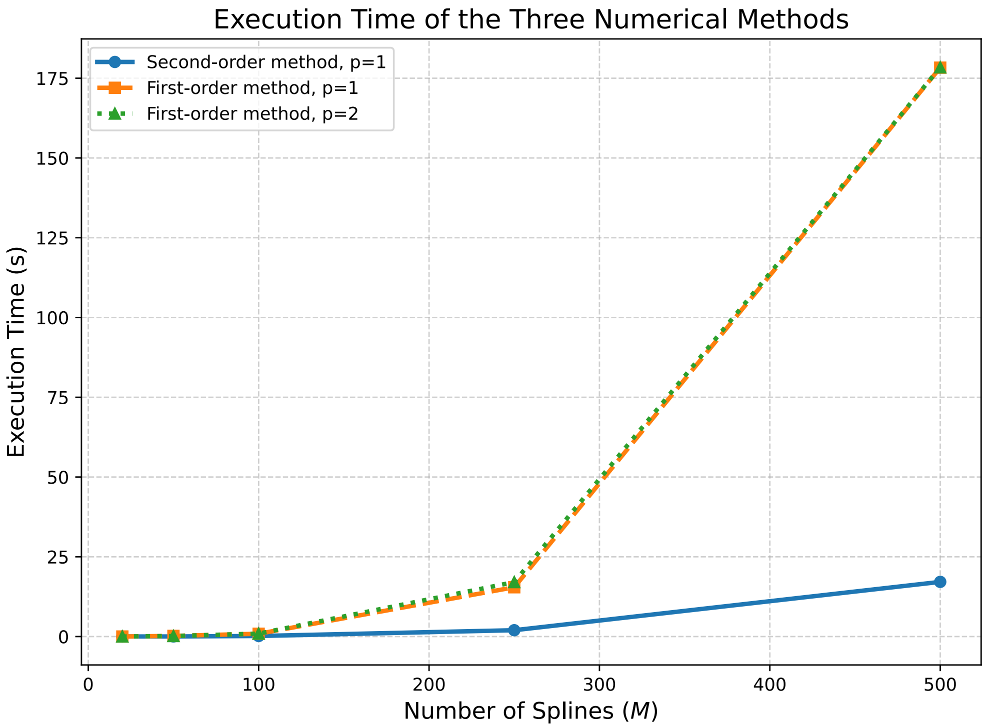

Figure 3.8: Comparison of execution times between the proposed direct second-order method ($p = 1$) and the augmented first-order method ($p = 1$ and $p = 2$) as a function of the number of splines M. The curves reflect the asymptotic eightfold computational savings achieved by the direct formulation due to the elimination of structural redundancies.

3.7 Scalability with System Dimension

To further validate the computational superiority of the direct formulation, we investigate the execution time as a function of the physical system dimension, n. This scalability analysis is particularly relevant for engineering applications, where modeling multi-body dynamics, spatially discretized partial differential equations, or complex interconnected networks naturally yields high-dimensional spaces.

For this experiment, the discretization mesh is kept constant at a relatively coarse resolution of $M = 20$. The parameter matrices $A, B, C, D \in \mathbb{C}^{n\times n}$ are generated as dense, random complex matrices—following the exact statistical methodology employed in the previous spectral distribution analysis—to prevent algorithmic shortcuts derived from matrix sparsity.

Figure 3.9 illustrates the computational time required by the direct second-order method ($p = 1$) and the augmented first-order methods ($p = 1$ and $p = 2$) as the matrix dimension n increases. The empirical results reveal a computational bottleneck for the augmented approach, whereas the direct method maintains a comparatively low execution time even for high-dimensional systems.

This behavior can be explained using the exact matrix dimensions derived in the previous section. Since the number of basis functions M is fixed, the total size of the discrete algebraic eigenvalue problem N scales linearly with the system dimension n. Recalling the $\mathcal{O}(N^3)$ complexity of the generalized eigenvalue solver, the theoretical execution times scale as $\mathcal{O}(n^3)$. However, the leading constant coefficient dictates the actual computational burden:

$$\mathrm{Cost}_{\mathrm{Direct}} \propto \big((M+4)n\big)^3 = (M+4)^3 n^3, \tag{3.13}$$

$$\mathrm{Cost}_{\mathrm{Augmented}} \propto \big(2(M+3)n\big)^3 = 8(M+3)^3 n^3. \tag{3.14}$$

Even for a fixed, small number of splines (e.g., $M = 20$), the structural redundancy of the augmented space forces the solver to process a matrix that is almost twice as large. When cubed, this topological inefficiency introduces a substantial performance penalty. As visually confirmed by the steep exponential-like curves in Figure 3.9, the augmented method rapidly becomes computationally prohibitive.

Consequently, the proposed direct second-order framework is not only more efficient for high-fidelity spectral approximations (large M) but is also better suited to large-scale delay differential equations (large n), where augmented first-order reformulations fail due to cubic scaling exhaustion.

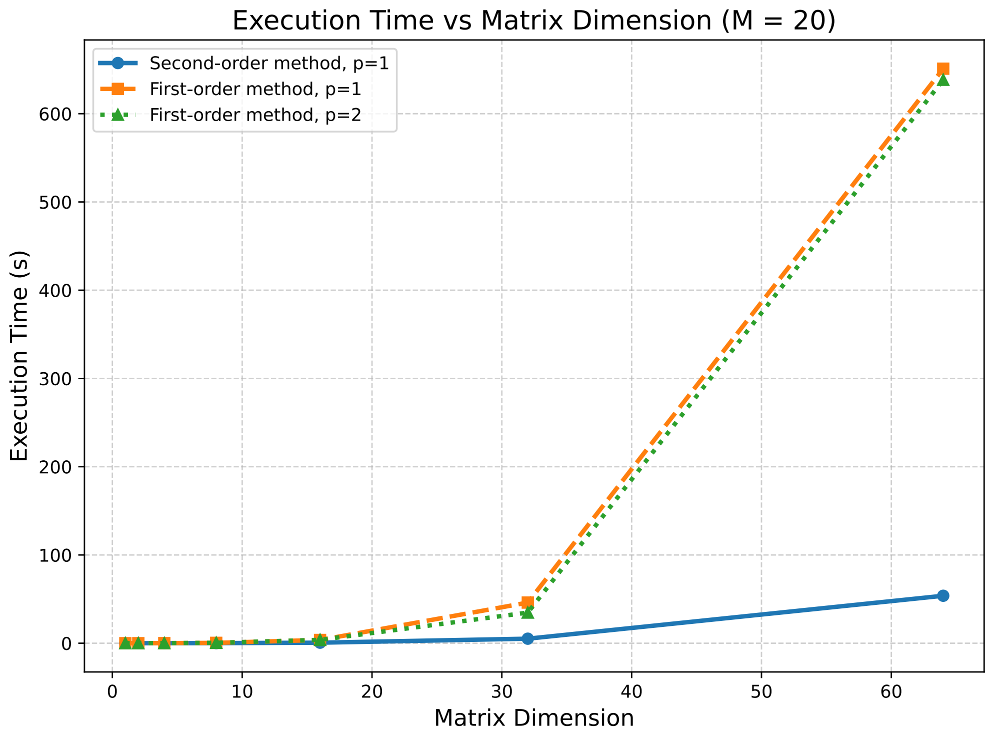

Figure 3.9: Execution time comparison between the direct second-order method and the augmented first-order method as a function of the physical system dimension n, evaluated at a fixed mesh size of $M = 20$. The divergence illustrates the $\mathcal{O}(n^3)$ penalty imposed by the duplicated space of the augmented formulation.

3.8 Spectral Purity and Spurious Eigenvalues

An inevitable algebraic consequence of the differing matrix dimensions is the total number of eigenvalues computed by the numerical solver. As established previously, for a given number of splines M, the direct second-order method generates a discrete system of size $N_{\text{Direct}} = (M+4)n$, while the augmented first-order method yields a system of size $N_{\text{Augmented}} = 2(M+3)n$. Because numerical eigenvalue algorithms strictly return a number of roots equal to the dimension of the input matrix, the augmented method inherently computes almost twice as many eigenvalues as the direct method.

This mathematical obligation introduces a critical qualitative difference between the two approaches: the generation of spurious (fictitious) numerical roots. In the augmented domain $D(A_0)$, the position and velocity states are treated as independent functional variables. Consequently, the Galerkin projection must expend high-frequency degrees of freedom to artificially enforce the kinematic constraint ($u_2 = u_1'$) across the delay interval. The supplementary eigenvalues generated by the augmented method are not physical modes of the dynamical system; rather, they are highly damped numerical artifacts representing the algorithm's effort to reconcile this structural redundancy.

Figure 3.10 visually corroborates this phenomenon by comparing the spectra obtained from both methods across multiple mesh resolutions ($M \in \{20, 50, 100, 250, 500\}$).

As shown in the detailed zoomed view (Figure 3.10b), both methods closely coincide in the immediate vicinity of the imaginary axis. For these dominant, low-frequency modes, the eigenfunctions are smooth, the kinematic constraint is easily satisfied, and both discretizations accurately capture the true physical stability of the system. However, observing the left side of the same zoomed view reveals the onset of the fictitious roots generated solely by the augmented method. These secondary eigenvalues appear exclusively as crosses, failing to coincide with any spectral points from the direct method. As the mesh resolution M increases, these spurious roots do not converge to any stable physical value; instead, they continuously drift across the complex plane, confirming their nature as non-physical numerical noise.

The global spectrum view (Figure 3.10a) further exposes the numerical pollution inherent to the augmented formulation. As the mesh is highly refined (e.g., $M = 500$, marked in purple), the direct second-order method (circles) produces a clean, bounded asymptotic arc. By contrast, the augmented first-order method (crosses) generates a large secondary arc of highly damped fictitious roots.

By embedding the exact kinematics directly into the definition of the infinitesimal generator A_2, the proposed direct method bypasses this numerical contamination. It provides a spectrally pure approximation that exclusively isolates the physically meaningful roots, ensuring that stability analyses are not compromised by drifting, high-frequency asymptotic artifacts.

3.9 Engineering Applications: The Machining Chatter Problem

To fully appreciate the computational advantages of the proposed direct second-order method, it is essential to contextualize the mathematical framework within a real-world engineering problem. While classical ordinary differential equations (ODEs) assume that a system's future evolution depends solely on its current state, physical reality is rarely instantaneous. In many natural and artificial systems, information, energy, or mass takes a finite amount of time to propagate. This temporal lag requires the introduction of "memory" into the dynamical model, naturally yielding Delay Differential Equations (DDEs).

In engineering, DDEs are ubiquitous. They govern biological population dynamics, traffic flow models, networked control systems with communication latency, and laser dynamics. However, an economically significant application of DDEs is found in manufacturing engineering: the prediction and avoidance of machine tool chatter.

3.9.1 The Regenerative Effect in Turning

During metal cutting processes, such as turning or milling, the machine tool and the workpiece form a complex dynamical system. Under certain operational conditions, the cutting process can become unstable, leading to self-excited vibrations known as *chatter*. Chatter causes poor surface finish, accelerated tool wear, unacceptable acoustic noise, and can even result in catastrophic failure of the machine components.

The accepted mechanism driving these instabilities is the *regenerative effect*, formalized in the mid-20th century by Tobias, Kudinov, and Tlusty. As illustrated in Figure 3.11, when a cutting tool removes material from a rotating workpiece, it leaves behind a wavy surface due to the structural vibrations of the machine. Exactly one revolution later, the tool cuts into this previously modulated surface. Consequently, the instantaneous cutting force depends not only on the current position of the tool but also on the position of the tool exactly one rotation ago. This physical delay, denoted as τ, is inversely proportional to the spindle speed.

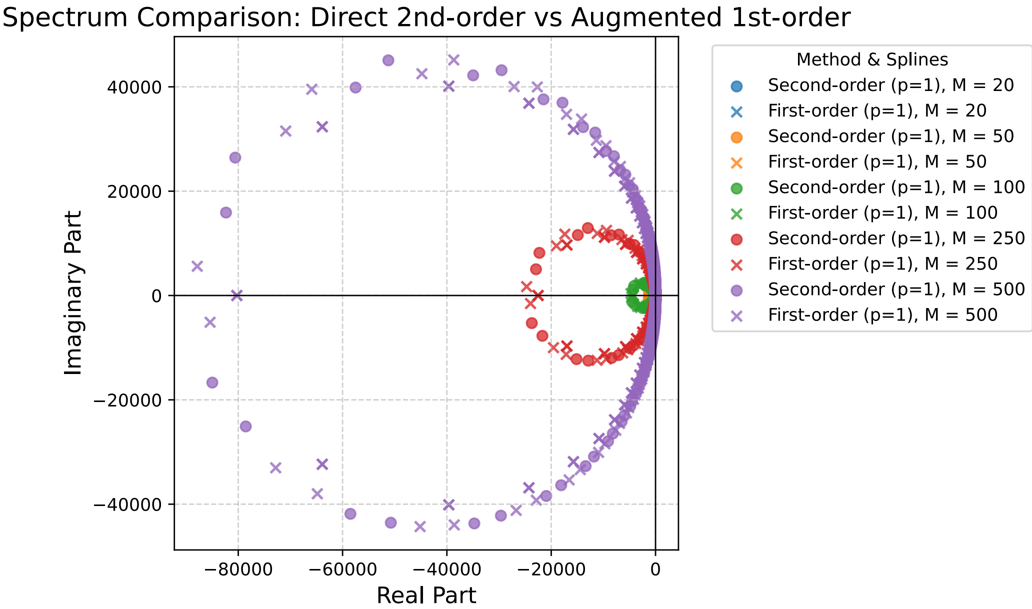

(a) Global spectrum view.

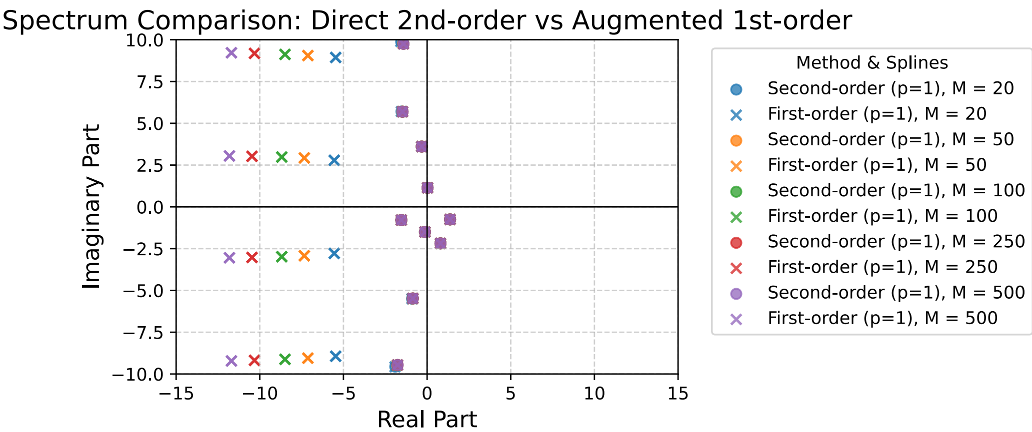

(b) Zoomed view near the origin.

Figure 3.10: Comparison of the computed spectra between the direct second-order method and the augmented first-order method. (a) The global view reveals a large outer arc of highly damped, spurious eigenvalues generated by the structurally redundant augmented formulation. (b) The zoomed view confirms that both methods closely coincide for the physically meaningful dominant roots near the imaginary axis. However, moving leftward, the augmented method exhibits secondary, fictitious eigenvalues (crosses) that do not coincide with the direct method and fail to converge to any physical mode as the mesh M increases.

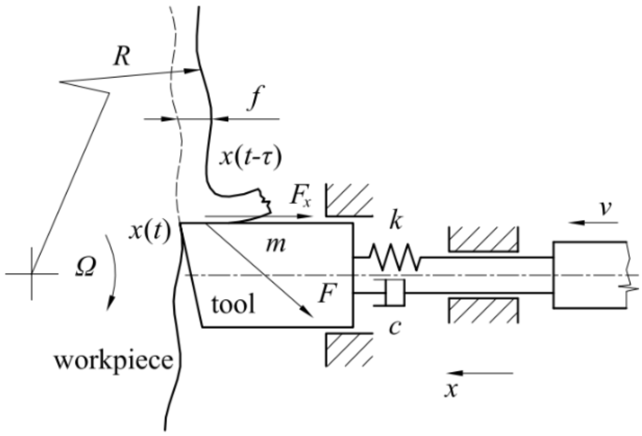

Figure 3.11: Mechanical model of the 1 degree-of-freedom (DOF) turning process. The instantaneous chip thickness $h(t)$ is determined by both the current displacement of the tool $x(t)$ and its delayed displacement $x(t-\tau)$ from the previous workpiece revolution. Adapted from Insperger and Stépán [2].

Following the foundational 1 degree-of-freedom (DOF) analysis by Insperger and Stépán [2], assuming a constant spindle speed Ω_0, the turning process can be mathematically modeled by a linear second-order DDE with a constant delay τ:

$$\ddot{x}(t) + 2\zeta\omega_n\dot{x}(t) + \omega_n^2 x(t) = -\frac{wh}{m}\big(x(t) - x(t-\tau)\big), \tag{3.15}$$

where ζ is the relative damping, ω_n is the natural angular frequency of the tool, w is the depth of cut, h is the specific cutting force coefficient, and m is the modal mass. Introducing dimensionless parameters, Equation (3.15) can be simplified to:

$$\ddot{x}(t) + 2\zeta\omega_n\dot{x}(t) + \omega_n^2 x(t) = -\tilde{w}\omega_n^2\big(x(t) - x(t-\tau)\big), \tag{3.16}$$

where $\tilde{w}$ represents the dimensionless depth of cut.

This formulation precisely mirrors the generic second-order DDE structure $\ddot{x}(t) + A\dot{x}(t) + Bx(t) = C\dot{x}(t-\tau) + Dx(t-\tau)$ targeted by our numerical method, where $A = 2\zeta\omega_n$, $B = \omega_n^2(1+\tilde{w})$, $C = 0$, and $D = \omega_n^2\tilde{w}$.

3.9.2 Validation: Computing the Stability Lobes

To validate the robustness and accuracy of the proposed direct second-order Galerkin projection, the method was deployed to solve Equation (3.16) and construct the classic stability chart for the turning process. Following the parameters used in [2], the relative damping was set to $\zeta = 0.02$, and the delay was defined as a function of the dimensionless spindle speed.

For the stability analysis, the continuous DDE was discretized using $M = 100$ basis splines. By scanning a comprehensive grid of dimensionless spindle speeds and depths of cut, the dominant eigenvalue (the root with the largest real part) was computed at each point. The boundary separating the stable cutting regime from the unstable chatter regime occurs exactly where the dominant eigenvalue crosses the imaginary axis ($\Re(\lambda) = 0$).

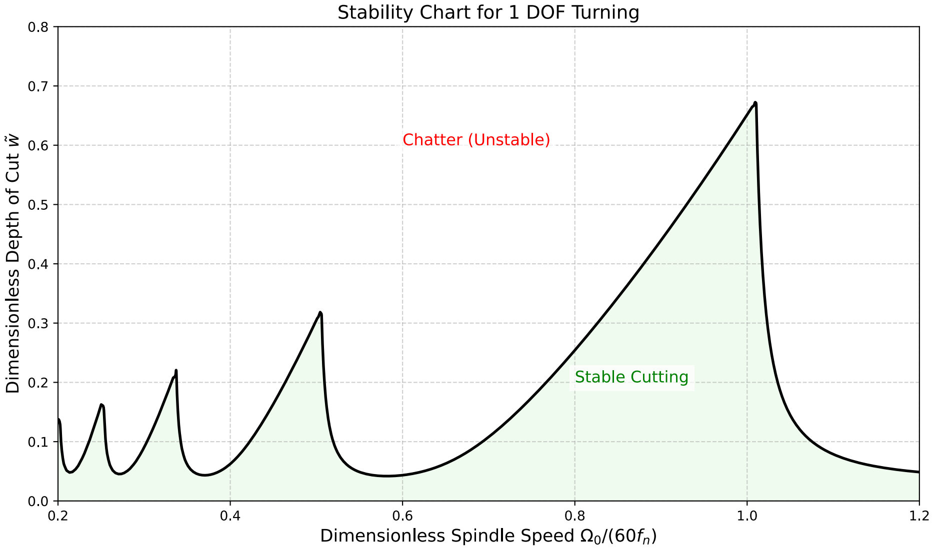

Figure 3.12: Stability chart for the 1 DOF turning process computed using the proposed direct second-order method. The solid black line represents the critical boundary where the dominant eigenvalue transitions from the left half-plane (Stable Cutting) to the right half-plane (Chatter), closely replicating the theoretical lobes described in [2].

As shown in Figure 3.12, the numerical results closely reproduce the characteristic “stability lobes” documented in the manufacturing literature. The direct method identifies the complex boundary geometry, without suffering from the numerical instability or spurious eigenvalue pollution that affects traditional augmented methods.

This reproduction not only validates the mathematical rigor of our algorithm but also highlights its direct applicability as a fast, reliable predictive tool for industrial machining optimization.

Chapter 4

Conclusions

4.1 Summary and Discussion of Results

Chapter 3 subjected the direct second-order Cayley-transform method developed in Chapter 2 to a systematic numerical evaluation. The first tests (Sections 3.1 and 3.2) confirmed, on a randomly generated test system, the two theoretical properties established in Lemma 2.4.1: the five genuinely unstable eigenvalues of the test system were correctly mapped outside the unit disk, while the infinite tail of highly damped roots was seen to accumulate at the point $\mu = -1$, exactly as predicted. The subsequent convergence study (Sections 3.2–3.4) revealed uneven behaviour across the spectrum: eigenvalues close to the imaginary axis—the ones that determine stability—converge rapidly and are essentially insensitive to the mesh size M, whereas eigenvalues deep in the left half-plane converge more slowly, a pattern that was observed consistently for every system dimension $n \in \{1, 2, 3, 4\}$ tested in Section 3.3.

The comparison against the augmented first-order method of Irastorza-Zabalegi and Ponce-Vanegas [4] (Sections 3.5–3.8) produced the main results of this work. In terms of accuracy, the two methods turned out to be equivalent when both use linear splines ($p = 1$): the marginal differences observed between them are case-dependent and cannot be attributed to the theoretical advantage of avoiding the augmented space. In terms of computational cost, however, the direct method was found to be substantially cheaper, since it operates on a space of dimension $N_{\text{Direct}} = (M + 4)n$ instead of $N_{\text{Augmented}} = 2(M + 3)n$, which—combined with the cubic cost of the generalized eigenvalue solver—yields an asymptotic eightfold reduction in execution time (Section 3.6), a gap that widens further with the system dimension n (Section 3.7). Moreover, the augmented formulation was shown in Section 3.8 to generate a large number of spurious, non-physical eigenvalues that do not converge to any true mode as M increases, a defect absent from the direct method. Finally, Section 3.9 applied the algorithm to the regenerative chatter problem in a one-degree-of-freedom turning process, reproducing the classical stability lobes of Insperger and Stépán [2] and confirming the practical applicability of the method beyond synthetic test cases.

4.2 Strengths of the Proposed Method

Two strengths of the proposed method stand out from the results of Chapter 3. The first is spectral purity: because the direct method embeds the kinematic relation between u and u' directly into the domain of the generator A_2, instead of imposing it weakly on an augmented, duplicated state as the first-order method does, it does not generate the spurious, fictitious eigenvalues documented in Section 3.8. Every eigenvalue produced by the direct method corresponds to a genuine mode of the original delay differential equation, which is a practical advantage when the method is used, as in Section 3.9, to scan a stability boundary automatically: there is no risk of a non-physical root being mistaken for the dominant one.

The second is computational efficiency: as shown in Sections 3.6 and 3.7, the direct method is asymptotically eight times faster than the augmented first-order approach for a fixed number of splines M, and it scales more favorably with the physical dimension n of the system. This efficiency gain comes at no cost in accuracy: for linear splines, Section 3.5 showed that the direct and augmented methods achieve equivalent convergence rates, so the reduction in computational cost is not a trade-off against precision but a direct gain, obtained simply by removing redundant degrees of freedom from the discretization. Together with the successful reproduction of the classical stability lobes in Section 3.9, this indicates that the method is not only theoretically sound but also directly usable on engineering problems, at a fraction of the computational cost of the existing approach.

4.3 Limitations and Difficulties

4.3.1 Limitations

The main limitation of the method, already anticipated in the discussion of Section 3.5, is that it does not improve the accuracy of the existing first-order approach: for linear splines, both methods converge at the same asymptotic rate and reach comparable error magnitudes for a given mesh size. The initial hypothesis that avoiding the augmented space would also improve precision, and not merely computational cost, was therefore not confirmed.

A second, more structural limitation is the poor convergence of the eigenvalues located far to the left of the imaginary axis, already identified in Section 3.2. The eigenfunctions associated with these highly damped roots behave like $e^{\lambda s}$ for $s \in [-\tau, 0]$ with $\Re(\lambda)$ strongly negative, and therefore develop a steep gradient close to the boundary of the delay interval. Since the linear splines used throughout this thesis are piecewise straight lines with a constant derivative on each element, they are structurally unable to reproduce such a steep slope unless the mesh is refined well beyond what is practical, and the resulting approximation error for these roots remains large even for the finest meshes considered. This effect is further amplified by the geometry of the inverse Cayley mapping, whose derivative $d\lambda/d\mu = 2/(\mu + 1)^2$ diverges precisely at the accumulation point $\mu = -1$ towards which these roots converge. As discussed in Section 3.2, this limitation does not compromise the practical use of the method for stability analysis, since it is the dominant, rightmost eigenvalues—for which convergence is fast and accurate—that determine the stability of the system.

4.3.2 Difficulties Encountered

Beyond the structural limitations of the method, the development of this work presented practical and theoretical challenges during both the mathematical formulation and the computational implementation phases.

The primary theoretical difficulty encountered in the early stages of this research was the definition of the semigroup T_2. Initially, T_2 was improperly defined, which led to theoretical inconsistencies and numerical results that were not coherent with the expected physical behavior. After thoroughly re-evaluating the underlying operator theory and boundary conditions, the correct formulation of the C_0-semigroup was identified. However, because the structural action and domain of the corrected semigroup differed from the initial formulation, a large portion of the codebase had to be refactored and rewritten to align with the revised theoretical framework.

From an algorithmic perspective, another hurdle concerned computational performance during matrix assembly. Both the construction of the mass matrix—which relies on the H^1 inner product used to orthogonalize the basis of $H_0^\perp$ (Section 2.5.3)—and the evaluation of the action of the modified Tustin operator on the spline basis (Section 2.4.1) involve path-dependent integrals of the form $\int_{-\tau}^{\theta} \psi(s)\, ds$. Evaluating all such integrals numerically at runtime every time an entry of the discretized matrices $\mathbf{A}$ and $\mathbf{B}$ was required would have made the algorithm prohibitively slow, particularly for the large mesh sizes M considered in Sections 3.6 and 3.7.

To overcome this bottleneck without sacrificing accuracy, a selective integration strategy was adopted based on exactness:

- Integrals that could be evaluated **exactly** using numerical quadrature were implemented directly using the Gauss quadrature method.
- Integrals that do **not** yield exact results under finite Gauss quadrature were solved analytically by hand. The resulting closed-form expressions were hard-coded directly into the implementation, ensuring the computer never performs non-exact numerical integrations at runtime.

This approach was not a minor detail, but a necessary condition for the computational feasibility of the method: without it, the direct formulation could not have achieved the eightfold efficiency gains reported in Section 3.6.

4.4 Concluding Remarks and Future Work

Overall, this thesis has shown that treating a second-order delay differential equation directly, without recasting it as an augmented first-order system, is a worthwhile strategy: it does not sacrifice accuracy with respect to the existing first-order Cayley-transform method of [4], it eliminates the spurious eigenvalues inherent to the augmented formulation, and it reduces computational cost by close to an order of magnitude, all while remaining directly applicable to an engineering problem such as the prediction of chatter in machining.

A natural direction for future work follows from the limitation discussed above. Since the poor convergence of the leftmost eigenvalues is a consequence of the limited flexibility of linear splines, the natural next step is to extend the current implementation to splines of higher degree ($p = 2$ and beyond), following the same route already available in the augmented first-order reference method (Section 3.5, Figure 3.7). Because higher-degree splines are no longer restricted to a piecewise-constant derivative, they can locally reproduce much steeper slopes, and should therefore improve the precision with which the highly damped, deep-left eigenvalues are recovered, at the price of a more involved—though still analytically tractable—derivation of the associated basis integrals. A complementary, less immediate alternative would be to concentrate the mesh non-uniformly near the endpoints of the delay interval $[-\tau, 0]$, where the boundary-layer behaviour responsible for this limitation is located, instead of refining the mesh uniformly as done throughout this work.

Bibliography

[1] Gene H. Golub and Charles F. Van Loan. *Matrix Computations*. Johns Hopkins University Press, Baltimore, MD, 4th edition, 2013.

[2] Tamás Insperger and Gábor Stépán. Chatter suppression of turning process via periodic modulation of the spindle speed: a 1 dof analysis. In *Proceedings of the Third Conference on Mechanical Engineering*, pages 720–724. Budapest, Hungary, 2002.

[3] Tamás Insperger and Gábor Stépán. *Semi-Discretization for Time-Delay Systems: Stability and Engineering Applications*, volume 178 of *Applied Mathematical Sciences*. Springer, New York, 2011.

[4] Markel Irastorza-Zabalegi and Felipe Ponce-Vanegas. The Tustin Method for approximating eigenvalues of delay systems. *Journal of Computational and Applied Mathematics*, 472:116772, 2026.

[5] Erwin Kreyszig. *Introductory Functional Analysis with Applications*. John Wiley & Sons, New York, 1978.

[6] Mark Lichtner, Matthias Wolfrum, and Serhiy Yanchuk. The spectrum of delay differential equations with large delay. *SIAM Journal on Mathematical Analysis*, 43(2):788–802, 2011.

[7] S. V. Lunel. Spectral theory for delay equations. In A. A. Borichev and N. K. Nikolski, editors, *Systems, Approximation, Singular Integral Operators, and Related Topics*, pages 465–507. Birkhäuser Basel, Basel, 2001.

[8] Amnon Pazy. *Semigroups of Linear Operators and Applications to Partial Differential Equations*, volume 44 of *Applied Mathematical Sciences*. Springer-Verlag, New York, 1983.